Helsinki University of Technology
Department of Chemical Technology
Laboratory of Physical Chemistry and Electrochemistry
Espoo 2003

Novel routes to metal nanoparticles:
Electrodeposition and reactions at liquid|liquid interfaces

Christoffer Johans

Dissertation for the degree of Doctor of Science in Technology to be presented with due permission of the Department of Chemical Technology, for public examination and debate in Auditorium Ke2 at Helsinki University of Technology (Espoo, Finland) on the 26$^{\text{th}}$ of April, 2003, at 12 noon.

ISBN 951-22-6467-6 (printed)
ISBN 951-22-6468-4 (URL: http://lib.hut.fi/Diss/)

Edita Prima
Helsinki 2003

Abstract

This thesis considers the nucleation and growth, synthesis, and catalytic application of metallic nanoparticles at liquid|liquid interfaces. It comprises five publications, a previously unpublished synthesis of polymer coated palladium nanoparticles, and an introduction to the relevant literature. Three publications are concerned with electrodeposition of metal nanoparticles at liquid|liquid interfaces. One publication and the results presented here consider the synthesis of silver and palladium colloids by reduction with pyrrole and thiophene monomers. The fifth publication demonstrates the use of gold and palladium colloids as electrocatalysts in two-phase dehalogenation reactions.

The literature reviewed serves as an introduction to nanoparticles, liquid|liquid interfaces and electrodeposition studies relevant to the publications and experimental studies presented herein. Nucleation models used are evaluated by numerical means.

In the electrodeposition studies, the fundamentals of deposition reactions at liquid|liquid interfaces, involving irreversible Butler-Volmer type growth kinetics and overlap of diffusion fields are developed. The importance of applied potential, particle agglomeration and surface activity on the nucleation process is shown.

Small metallic nanoparticles were synthesized in homogeneous media, using novel syntheses involving pyrrole and thiophene derivatives as both reductants and stabilizators.

The use of aqueous metal colloids as catalysts for dehalogenation reactions in a two-phase immiscible electrolyte system is demonstrated. Specifically palladium or gold colloids prepared by the citrate reduction method can be negatively charged in a heterogenous two-phase reaction with decamethylferrocene, and subsequently used as an aqueous catalyst for dehalogenation of 2-bromoacetophenone.

Preface

This work was carried out at the Laboratory of Physical Chemistry and Electrochemistry, Helsinki University of Technology, Finland from March 1999 to November 2001, and continued at home until October 2002. Part of the work was conducted at the University of Limerick, Ireland 13.6.2001-31.7.2001.

I wish to express my gratitude to the head of the laboratory, professor Kyösti Kontturi, for the supervision of my studies and interest in my work. I would also like to thank emeritus professor Göran Sundholm and professor Simo Liukkonen for their guidance of my studies. The invaluable contributions by professor D. J. Schiffrin and professor Vincent Cunnane have been most welcome. Professor Alan C. West is thanked for numerical simulation results. Dr. Ritva Serimaa is acknowledged for the X-ray diffraction analysis.

Research colleagues and permanent staff in the Laboratory of Physical Chemistry and Electrochemistry are thanked for a helpful and encouraging working atmosphere. Dr. Peter Liljeroth's and Dr. Bernadette Quinn's never ceasing ideas and interest have been welcome. I would also like to thank Dr. Riikka Lahtinen, Sanna Hakkarainen, Jason Clohessy and Sebastien Fantini for fruitful collaboration.

I want to express my gratitude to Laura for her endless patience and support.

The financial support of the Academy of Finland through the ESPOM (Electrochemical Science and Technology of Polymers and Membranes) graduate school as well as the National Technology Agency (Finland) is gratefully acknowledged.

Contents

List of Publications

I C. Johans, R. Lahtinen, K. Kontturi, D. J. Schiffrin, Nucleation at liquid|liquid interfaces: Electrodeposition without electrodes. J. Electroanal. Chem., 488 (2000) 99–109.

II C. Johans, K. Kontturi, D. J. Schiffrin, Nucleation at liquid|liquid interfaces: Galvanostatic study, J. Electroanal. Chem., 526 (2002) 29–35.

III C. Johans, P. Liljeroth, K. Kontturi, Electrodeposition at polarisable liquid|liquid interfaces: The role of interfacial tension on nucleation kinetics, Phys. Chem. Chem. Phys., 4 (2002) 1067–1071.

IV C. Johans, J. Clohessy, S. Fantini, K. Kontturi, V. J. Cunnane, Electrosynthesis of phenylpyrrole coated silver particles at a liquid-liquid interface, Electrochem. Commun., 4 (2002) 227–230.

V R. Lahtinen, C. Johans, S. Hakkarainen, D. Coleman, K. Kontturi, Two-phase electrocatalysis by aqueous colloids, Electrochem. Commun., 4 (2002) 479–482.

This thesis also includes previously unpublished work regarding the synthesis of palladium nanoparticles from palladate and thiophene-3-acetic acid.

Statement on the author's role in listed publications

In the case of papers I and II, Christoffer Johans has done all experimental and theoretical work. He has also been the principal author of these papers. Christoffer Johans has done all experimental work included in paper III. The theory presented in paper III and manuscript preparation was undertaken jointly with Peter Liljeroth. In paper IV, Christoffer Johans has done the principal experimental work and was the principal author of the paper. In paper V, Christoffer Johans has actively participated in the planning of the experiments, evaluation of experimental results and writing of the paper.

In addition to these papers, the thesis contains unpublished results on the synthesis of thiophene-3-acetic acid stabilized palladium nanoparticles.

Espoo, 5.11.2002

Kyösti Kontturi
Professor

1 Introduction

The history of metal nanoparticles begins with Faraday's study of gold colloids. However, it was not until Feynman's revolutionary insights on quantum electrodynamics [1] and the recent advent of microscopic techniques with subnanometer resolution that nanomaterial research has become increasingly popular. A computer search through the chemical abstracts reveals that more than 5000 articles concerning nanoparticles have been published in international journals during just 2002, which demonstrates the popularity of this topic. The growing interest and importance stem from the various unique applications [2–6] that nanoparticles can be used for, such as catalysts [7], oligonucleotide recognition [8], electronic [9] and optical components [10].

The properties of nanoparticles gradually change from those of bulk material to molecular with decreasing particle size. In the intermediate range, materials with novel properties, exhibiting characteristics typical for both molecular and bulk materials are found. These materials are used to bridge the gap between the macroscopic and the microscopic world in many applications. However, applications that benefit from nano-properties require particles with well-defined size, shape and surface properties. The greatest obstacle for the implementation of nano-devices today is the lack of techniques for mass production and assembly of nanoparticles. Neither conventional methods of controlling bulk materials nor common chemical synthetic methods are suitable for nanomaterials. These require a delicate balance between the physical forces, usually defined by their surface properties, that determine their behavior. The two main approaches for building nano-devices are the "top down" and "bottom up". In the former, nano-devices are built by miniaturization of conventional techniques, such as lithography. In the latter, nanoparticles are used as building blocks, which are assembled in a controlled fashion.

In order to synthesize well-defined monodisperse nanoparticles, control over the nucleation and growth process is essential. There are several different methods for making nanoparticles. The most common approach is based on the use of a suitable capping agent, that passivates growth at an early stage. Other techniques include laser ablation and gas phase nucleation from

metal vapor. Electrochemistry offers an interesting method, as the supersaturation and hence the growth conditions can be directly monitored with the applied potential [11]. This is especially efficient for studying the formation and growth of nanoparticles. However, the nucleation process at a solid electrode is affected by the interaction between the newly formed phase and the electrode substance. The main difference when nucleation takes place at a liquid|liquid interface is that, for the latter, this interaction is very small. In this respect, the liquid|liquid interface is ideal for nucleation studies.

This thesis presents three publications on electrochemical nucleation at liquid|liquid interfaces, one publication concerning the synthesis of nanoparticles with conducting polymers and one publication demonstrating the use of a metal colloid as an electrocatalyst in an immiscible liquid|liquid system. The literature part introduces nanoparticles, electrodeposition and liquid|liquid interfaces, and relates the work done in this thesis to contemporary research. More specifically, chapter 2 briefly presents properties and synthesis of metal nanoparticles. Chapter 3 introduces liquid|liquid interfaces, and in chapter 4, electrodeposition is discussed. Additionally, a novel method for Pd nanoparticle synthesis is presented in chapter 5.

2 Metallic nanoparticles

Preparation of metallic colloids dates back to the middle ages [12], however, the nature of these colloids remained unclear, until Faraday realized that the gold colloids he studied contained small metallic particles, which he called divided metals [13]. In recent years, the term "nanoparticle" has evolved. A nanoparticle has dimensions in the nanometer range, *i.e.* between 0.5 and 100 nm. The term colloid is more elusive, the particle size can range from nanometers to several hundreds of micrometers. Additionally, a colloid implies that the particles are dispersed in a medium, and do not separate on long standing. The term cluster is usually used for small nanoparticles that have well-defined composition and surface structure.

There has been steady progress in understanding the nature and properties of nanoparticles, especially during the last two decades. Many reviews have been published on general properties and structures of clusters and colloids [2–7, 14, 15].

Nanoparticles cannot simply be treated as minute blocks of a metal, as implied by the term divided metals. In bulk metals, the large density of states at the Fermi level forms a conduction band of continuous energy levels. However, as the particle size decreases, the valence electrons become confined, and hence, discrete energy levels occur. This phenomenon is called the size-induced metal-insulator transition. It is a gradual change that occurs over a range of sizes, typically, at ambient temperature, clusters of 13 atoms are non-metallic, while clusters of 309 atoms and larger show distinct bulk metal properties [3]. The metal-insulator transition is readily observed through changes in electronic, optical and catalytic properties. Generally, the loss of metallic character also results in loss of catalytic activity [16].

The magic numbers of nuclearity, *i.e.* 13, 55, 147, 309, 561 provide energetically favorably geometries associated with closed-shell structures, resulting in a sequential series of particle sizes centered around the magic numbers [14].

The fraction of surface atoms increases dramatically with decreasing particle size. A nanoparticle of 3 nm would have $\sim$45% of the atoms on the surface, compared to $\sim$76% for a 1 nm particle. Surface atoms play an espe-

cially important role in catalysis, as the reaction takes place at the surface of the particle. Furthermore, larger surface area increases the relative contribution of the surface energy, and therefore the thermodynamic stability is decreased with decreasing particle size. In nucleation studies, this phenomenon is observed as a nucleation overpotential, determining the kinetics of nucleation processes, and is discussed further in chapter 4.

The crystal structure of metal nanoparticles is also of interest. High resolution transmission electron microscopy (HRTEM) shows that small particles in the 1 to 2 nm range also adopt a cuboctahedral shape corresponding to bulk crystal structure [17], however, with relaxation of the lattice dimension due to the large fraction of surface atoms. Normally larger particles are polycrystalline, though monocrystalline can also be observed [3].

2.1 Preparation of metallic nanoparticles

A large variety of synthetic methods for nanoparticles have been developed. Recently, the emphasis of synthesis has been on the preparation of monodisperse particles, with well-defined size, shape and surface properties. Control over these parameters is crucial for a successful utilization of the size-dependent properties that are unique to nanoparticles, and is particularly important in assembly of monolayer protected nanoparticles into crystalline arrays of one-, two- or three-dimensions. Such assemblies are of interest for future generation nanoelectronics [18]. Particles intended as catalysts are generally not sensitive to the particle size, however, the particle surface must be readily available to the reactant, and thus, any protective agents that are used must not adsorb too strongly [19].

Metal nanoparticles have been prepared by a wide variety of techniques such as laser ablation [4], nucleation from vapor [20], thermal decomposition of organometallic compounds [21–24], sonolysis [25, 26], pulse radiolysis [27], electrochemical reduction [28–30] and chemical reduction of the corresponding metal salts.

Reduction of metal salts in the presence of a suitable protecting agent is the most commonly used technique. Generally, a reductant, such as borohydride, hydrotriorganoborates [31], hydrogen or citrate [32], is added to a solution of the corresponding metal salt. An easily oxidized solvent may

function both as the electron donor and the dispersing medium. Such particles are of particular interest for catalysis, as the metal surface is readily accessible. Alcohols and ethers have been quite extensively used for this purpose [19, 33].

Metal nanoparticles have a tendency to agglomerate, and therefore, it is necessary to protect them using surfactants or polymers, such as cyclodextrin [34], PVP [35], PVA [33,36,37], citrate [32,38] or quaternary ammonium salts [28–30, 39]. In another strategy, the metal salt is reduced in micelles [40, 41]. In this technique, the micelles function as nanoreactors, where the size of the particles can be controlled by the concentrations used and the micelle size.

Schiffrin *et al.* [42–44] presented a technique that produces small alkanethiolate protected nanoparticles. In this reaction, nanometer sized gold particles are prepared by mixing an aqueous solution of tetrachloroaurate with a toluene solution of a tetra-alkyl ammonium salt and an alkane thiol, followed by the addition of a borohydride solution. The tetra-alkyl ammonium salt functions as a phase transfer agent for $[AuCl_4]^-$. The resulting particles differ from conventional colloids in that they can be repeatedly isolated from and redissolved in common organic solvents without irreversible aggregation or decomposition. The particles can be crystallized in size fractions by a suitable choice of solvent pairs. These particles can store charge by injection or ejection of electrons [5]. This charging phenomenon is formally analogous to the classical STM-based Coulomb staircase [45]. Additionally, the thiol ligands may be exchanged for functionalized thiols, allowing flexible variation of the properties and the use of the particles as building blocks in chemistry. This synthesis has become very popular and reference [42] is the most cited paper in Chemical Communications to date.

Although the size of nanoparticles cannot be exactly controlled during synthesis, it is possible to narrow the size distribution by controlling the reaction conditions. Complete control over the size distribution requires size selection techniques, such as size-selective precipitation [46–48]. This method is based on a so-called solvent/non-solvent pair, that are mutually miscible, but differ in their ability to dissolve the particles. The particles can be precipitated by varying the ratio of the solvents. The method is applicable only to reversibly precipitative particles.

3 The interface between two immiscible electrolyte solutions

The first electrochemical experiment at an interface between two immiscible electrolyte solutions (ITIES) was conducted already 1902 by Nernst and Reisenfeld [49]. Since then, electrochemistry at liquid|liquid interfaces has become a well-established area of research. An important step in the development of ITIES was achieved in 1953, when Karpfen and Randles [50] presented an analysis of the thermodynamic equlibrium between the two phases and thereby laid the foundation for further work. The breakthrough in experimental studies at ITIES came 1968 when Gavach *et al.* [51] proved that the interface between two electrolyte solutions could be polarized if a hydrophilic electrolyte was chosen for the aqueous and a hydrophobic electrolyte for the organic phase. They also demonstrated that a charge transfer reaction between the two phases could be obtained by imposing a Galvani potential difference.

Several studies on bio-related systems, such as biomembrane mimetics [52–54], and pharmacokinetic characterization [54–63] have been undertaken due to the similarities between liquid|liquid interfaces and a half of a biological membrane. Other applications include solar energy conversion [64–66], metal extraction [67–69], catalysis [70–73], deposition reactions [11, 74–76] and electroanalysis [77–82]. Most electrochemical techniques developed for the solid electrode|electrolyte interface can be applied to liquid|liquid interfaces.

This chapter presents an introduction to the liquid|liquid interface, more specifically to the interfacial structure, ion transfer, electron transfer, reactions and catalysis, and electrodeposition at liquid|liquid interfaces. These concepts are of importance to all publications included in this thesis.

3.1 Structure and properties of liquid|liquid interfaces

Understanding electrochemical reactions at liquid|liquid interfaces requires knowledge of the structure of the interface. Liquid|liquid interfaces differ from the solid|electrolyte interfaces in many aspects. The former are dynamic

structures that change constantly, while solid interfaces usually have a well-defined boundary, *i.e.* they are molecularly sharp also on long time scales. At the liquid|liquid interface, molecular sharpness is not self-evident and partial mixing in the interfacial region cannot be excluded.

Relatively few experimental techniques exist by which the structure of a liquid|liquid interface can be probed with molecular level resolution. Much of the knowledge gathered to date is based on molecular dynamics simulations.

The structure of liquid/liquid interfaces has been assessed by X-ray reflectivity measurements [83–85]. A width of 0.33 nm for an alkane/water interface was calculated from the electron density profile. Within the context of capillary wave theory, this is in agreement with macroscopic measurements of the interfacial tension. Strutwolf *et al.* [86] measured the surface roughness of a water|1,2-dichloroethane interface by neutron scattering, and found it to be less than 1 nm, which also is in accordance with that predicted by capillary wave theory. Trojanek *et al.* [87] used a laser beam to measure the scattering from capillary waves at a polarized water|1,2-DCE interface. The interfacial tension calculated from the capillary waves corresponds well to that obtained for the interfacial tension measured by conventional methods. The liquid|liquid interface has also been studied by second harmonic generation (SHG) [88–92] and sum frequency generation (SFG) [93–99]. These techniques are surface specific, and yield information on concentrations and orientations of adsorbed species.

Benjamin *et al.* have studied the interfacial structure through molecular dynamics simulations [100–107] showing that although the water|1,2-DCE interface is molecularly sharp, the interface undergoes constant change with "fingers" of one phase penetrating into the other. These fingers are ca. 0.8 nm long with a lifetime of 10^{-13} s at room temperature. The simulations also show that the water molecules in the interfacial layer have a mean orientation, contrary to bulk phase. Molecular dynamics simulations are limited in that contemporary computers are not fast enough to incorporate sufficiently large numbers of ions and solvent molecules in the calculations to describe a polarizable liquid|liquid interface appropriately.

The first capacitance model for the liquid|liquid interface was developed long before any detailed electrochemical studies of the polarized liquid|liquid

interface had been made. This model was a generalization of the Gouy-Chapman model, accounting for the diffuse double layers in the two adjoining phases [108]. A modification of this model, incorporating ion-free inner layers in the interfacial region of the respective phases, was presented by Gavach *et al.* [109]. This concept is well established for solid electrodes as the Stern-Gouy-Chapman model. Neither the model by Vervey and Niessen nor the model by Gavach *et al.* are able to reproduce experimental capacitance data accurately. Samec *et al.* [110, 111] proposed a further modification of the modified Vervey-Neissen model, that accounted for the penetration of ions into the inner layer.

In the model by Girault and Schiffrin [112], the properties of the two liquids were gradually allowed to change in a mixed solvent layer. In view of MD simulations, laser, X-ray and neutron scattering experiments, the mixed solvent layer with microscopic mixing of the solvents does not appear likely. However, if the structure is averaged over longer time scales, a gradual change of the solvent properties in the interfacial region is obtained.

Schmickler *et al.* [113–117] presented a lattice gas model for the interfacial region of the liquid|liquid interface. Their simulations showed that the capacitance increases for ions that penetrate more easily across the interface, due to the overlap between the space charge regions. Additionally, it was shown that the interfacial region is enriched by ion pairs when the interface is polarized. Good qualitative agreement was found with experimental data.

3.2 Ion transfer across the liquid|liquid interface

The liquid|liquid interface differs from the usual solid|electrolyte interface in that the faradaic current due to charge transfer is not limited solely to electron transfer. Ions readily cross the interface, and commonly, the polarizability of the liquid|liquid interface is limited by transfer of base electrolyte ions. The energy needed to drive an ion from one phase into the other can be provided by applying a suitable potential difference across the interface. The standard ion transfer potential, $\Delta_{\mathrm{o}}^{\mathrm{w}}\phi_{\mathrm{i}}^{0}$, reflects the difference in the solvation

energy, $\Delta_{\mathrm{o}}^{\mathrm{w}}G_{\mathrm{i}}^{0}$, of the ion in the respective phases [118]:

$$\Delta_{\mathrm{o}}^{\mathrm{w}}\phi_{\mathrm{i}}^{0} = \frac{\mu_{\mathrm{i}}^{0,\mathrm{o}} - \mu_{\mathrm{i}}^{0,\mathrm{w}}}{z_{\mathrm{i}}F} = \frac{\Delta_{\mathrm{o}}^{\mathrm{w}}G_{\mathrm{i}}^{0}}{z_{\mathrm{i}}F} \tag{1}$$

where i refers to the ion under consideration, z_{i} is the charge of the ion and μ_{i}^{0} is the chemical potential in the respective phase. The TATB assumption has been introduced as a reference state for the energy scale [119]. This assumptions states that $TPAs^{+}$ (tetraphenylarsonium) and TPB^{-} (tetraphenylborate), which have similar structures but opposite charges, have equal transfer energies between an aqueous and an organic phase.

All interfaces can be classified between the limits of ideally polarizable and ideally non-polarizable. If ions of the same species are present in both phases, the liquid|liquid interface approaches a non-polarizable interface, *i.e.* a small perturbation from the equilibrium potential results in a large current. A common ion, also called a potential determining ion [72, 109], can be used to set the potential difference without external potential control. If, on the other hand, non-partitioning salts, *i.e.* hydrophobic and hydrophilic salts are chosen for the organic and aqueous phase electrolytes, respectively, the liquid|liquid interface approaches ideal polarizability. However, in practice the transfer energy of the base electrolyte ions determine the potential range in which the interface can be polarized. This range, the so-called potential window, is usually limited to 400-700 mV depending on the organic solvent, the electrolytes and their concentrations.

There are two main types of ion transfer. The first type, normally referred to simply as ion transfer, involves only resolvation and transfer of an ion from one phase to the other phase. In the second type, facilitated ion transfer, the transferring ion forms a complex with a ligand from the opposite phase at the interface, *e.g.*

$$\mathrm{X}^{z}(\mathrm{aq}) + n\mathrm{L}(\mathrm{o}) \rightleftharpoons [\mathrm{XL}_{n}]^{z}$$

This complex then diffuses into the bulk. The formation of the complex lowers the energy needed for the transfer reaction. Facilitated ion transfer has been used for, *e.g.* ion-selective electrodes [120]. Facilitated ion trans-

fer can be divided into several categories depending on the details of the mechanism [121–126].

The kinetics of ion transfer has attracted much interest. Usually, a Butler-Volmer formalism has been employed. Early ion transfer studies [127–129], lacking suitable equipment and experimental techniques, gave quite low rate constants in the order of $k^0 \approx 10^{-4}$ cm s^{-1}. More recent studies [130–132] indicate that the ion transfer reaction is much faster, $k^0 > 10^{-1}$ cm s^{-1}.

3.3 Heterogeneous electron transfer at liquid|liquid interfaces

Contrary to a solid electrode where the electron conducting electrode substrate can donate or accept electrons, at a liquid|liquid interface both an electron donor and acceptor must be present in the opposing phases. The electron transfer can only occur directly between these two species. The electron transfer reaction from redox couple 1 in the aqueous phase and redox couple 2 in the organic phase can be written as [118]:

$$a\mathrm{Ox}_1(\mathrm{w}) + b\mathrm{Red}_2(\mathrm{o}) \rightleftharpoons a\mathrm{Red}_1(\mathrm{w}) + b\mathrm{Ox}_2(\mathrm{o}) \qquad \text{(I)}$$

where Ox denotes the oxidized and Red the reduced form of the respective redox couples. a and b are defined by the stoichiometry of the reaction. The equilibrium potential for this reaction can be derived from the Nernst equation and is given by [72]:

$$\Delta_{\mathrm{o}}^{\mathrm{w}}\phi = E^0_{\mathrm{Ox}_2/\mathrm{Red}_2} - E^0_{\mathrm{Ox}_1/\mathrm{Red}_1} + \frac{RT}{n_1 n_2 F} \ln \frac{a^a_{\mathrm{Ox}_1} a^b_{\mathrm{Red}_2}}{a^a_{\mathrm{Red}_1} a^b_{\mathrm{Ox}_2}} \qquad (2)$$

where n_1 and n_2 are the number of electrons transferred by the respective redox couples. E^0_{i} is the standard redox potential for the respective redox couples.

The phenomenological Butler-Volmer formalism has been used to describe electron transfer kinetics also at liquid|liquid interfaces [118]. In this model

the overall flux J is given by:

$$J = k_{\mathrm{f}} c^{\mathrm{w}}_{\mathrm{Red}_1} c^{\mathrm{o}}_{\mathrm{Ox}_2} - k_{\mathrm{b}} c^{\mathrm{w}}_{\mathrm{Ox}_1} c^{\mathrm{o}}_{\mathrm{Red}_2} \tag{3}$$

where k_{f} and k_{b} are the reaction rate constants for the forward and reverse reactions. The potential dependencies of the rate constants are given by [118]:

$$k_{\mathrm{f}} = k^0 \exp \frac{-\alpha n F(\Delta^{\mathrm{w}}_{\mathrm{o}}\phi - \Delta^{\mathrm{w}}_{\mathrm{o}}\phi^0_{\mathrm{e}})}{RT} \tag{4}$$

and:

$$k_{\mathrm{b}} = k^0 \exp \frac{(1-\alpha) n F(\Delta^{\mathrm{w}}_{\mathrm{o}}\phi - \Delta^{\mathrm{w}}_{\mathrm{o}}\phi^0_{\mathrm{e}})}{RT} \tag{5}$$

where $\Delta^{\mathrm{w}}_{\mathrm{o}}\phi$ is the applied potential, $\Delta^{\mathrm{w}}_{\mathrm{o}}\phi^0_{\mathrm{e}}$ is the equilibrium potential of the reaction, k^0 is the standard rate constant and α is the transfer coefficient. The Butler-Volmer formalism works well for small overpotentials, but fails to describe the rate at high driving force.

The Marcus electron transfer theory was initially generalized for the liquid|liquid interface by Samec [133]. This model predicts that the electron transfer rate decreases at sufficiently high overpotentials. This phenomenon is referred to as the inverted region. Girault and Schiffrin [134] considered the electron transfer reaction as a series of steps, where the formation of a precursor complex of the reactants is followed by reorganization of the precursor, electron transfer and dissociation of the products. Marcus [135–138] has considered electron transfer at both molecularly sharp and interfaces with mixed solvent regions. Benjamin and Kharkats [139] generalized the Marcus theory for the case where the reactants can partition into the opposite phase. Electron transfer has also been approached by molecular dynamics [103, 139, 140] and lattice gas models [141]. The lattice gas approach indicated that the Gibbs energy of the reaction is only weakly dependent on the applied potential and that the major changes occur in the reactant concentrations in the interfacial region.

Although, there have been numerous experimental studies of electron transfer at liquid|liquid interfaces and several techniques have been applied, it cannot be clearly stated which electron transfer theory describes the experiments best. This is mainly due to the unknown structure of the interface

and the difficulty of finding suitable experimental systems, where the electron transfer and the species involved in the reaction are not accompanied by decomposition of the products, ion pairing, precipitation, or association with other species [142]. It is has, however, been found that Butler-Volmer kinetics are satisfactory at small overpotentials [143]. Also, the existence of the inverted region in electron transfer reactions at liquid|liquid interfaces has been reported [144].

3.4 Catalysis and reactions at liquid|liquid interfaces

The liquid|liquid interface offers interesting opportunities for catalysis due to an anisotropic environment, and a combination of aqueous and organic solvents, allowing for reactions between species of greatly different solubility. Catalysis at liquid|liquid interfaces can be classified into two main categories. In the first, polarization of the liquid|liquid interface transfers a reactant into the opposite phase where it subsequently reacts. This is *in principle* equivalent to phase transfer catalysis (PTC), where a so-called phase transfer salt is added to carry the reactants across the interface, and many PTC reactions used in organic chemistry can be explained by a common ion that sets the interfacial potential between the two phases [72]. Tan *et al.* [145] used the liquid|liquid interface to study the Williamson ether synthesis. Kong *et al.* [146] studied S_N2-substitutions of 1-toluenesulfonyl-2,4-dinitronaphthalene with hydroxide ions at the water|nitrobenzene interface. Forssten *et al.* [147] used the liquid|liquid interface to transfer MnO_4^- into the organic phase where it then oxidized cyclo-octene. Forssten *et al.* [148] have also investigated S_N2-substitutions of haloalkanes.

In the second category, the anisotropic interfacial environment promotes the reaction. There are relatively few examples where the anisotropic environment is directly related to the catalytic action. Lahtinen *et al.* [66, 70] showed photoreduction of benzoquinones and that electrodeposited palladium nanoparticles act as mediators for photocatalytic electron transfer reactions. Lahtinen [149] also showed that 1-octanol can be photochemically oxidized at the liquid|liquid interface. In these reactions, the anisotropic environment quenches the recombination of products resulting from the photochemically activated reactants.

Quinn *et al.* [150] have studied the redox reaction between an aqueous redox couple and alkane-thiol stabilized gold nanoparticles in an organic phase by scanning electrochemical microscopy (SECM). Interestingly, the electron transfer reaction was found to be slow, which was attributed to exclusion of the hydrophobic particles from the interfacial region.

Publication V presents a combination of two-phase catalysis, colloid catalysts and electrocatalysis. The advantage of this type of system is the facile separation of the catalyst and the reaction products. Aqueous gold and palladium colloids prepared by citrate reduction were used. It was shown by cyclic voltammetry that the colloids can be charged with electrons originating from decamethylferrocene (DcMFc) in the organic phase. The charging was also followed by electrophoretic light scattering measurements. The mobility, and hence, the negative charge on the particles increased with increasing DcMFc concentration. In the dehalogenation reaction the substrate, 2-bromoacetophenone, resides in the organic phase where mediated by the metal particles, it is reduced by decamethylferrocene, see Figure 1. A proton replaces the bromine leaving group. Two electrons are required in the reaction, one for the reduction of the proton and one for the bromine. Since the protons and the bromide readily transfer across the liquid|liquid interface at the applied potential, a positive net charge flows from the aqueous to the organic phase. Thus, the reaction is thermodynamically favored by positive potentials greater than 100 mV. A similar dehalogenation reaction has also been studied by Cheng and Schiffrin [73].

3.5 Electrodeposition at liquid|liquid interfaces

Electrochemistry offers an indispensable tool for investigating electrodeposition reactions, since the supersaturation can be controlled by the applied potential. Consequently, solid electrodes have been quite extensively used to study deposition reactions. However, only a few studies have so far been conducted at the polarizable liquid|liquid interface. The scientific interest to study deposition reactions at liquid|liquid interfaces lies in the absence of strong interactions between the newly formed phase and the electrode substrate. In this respect, the liquid|liquid interface should be more ideal than solid electrodes.

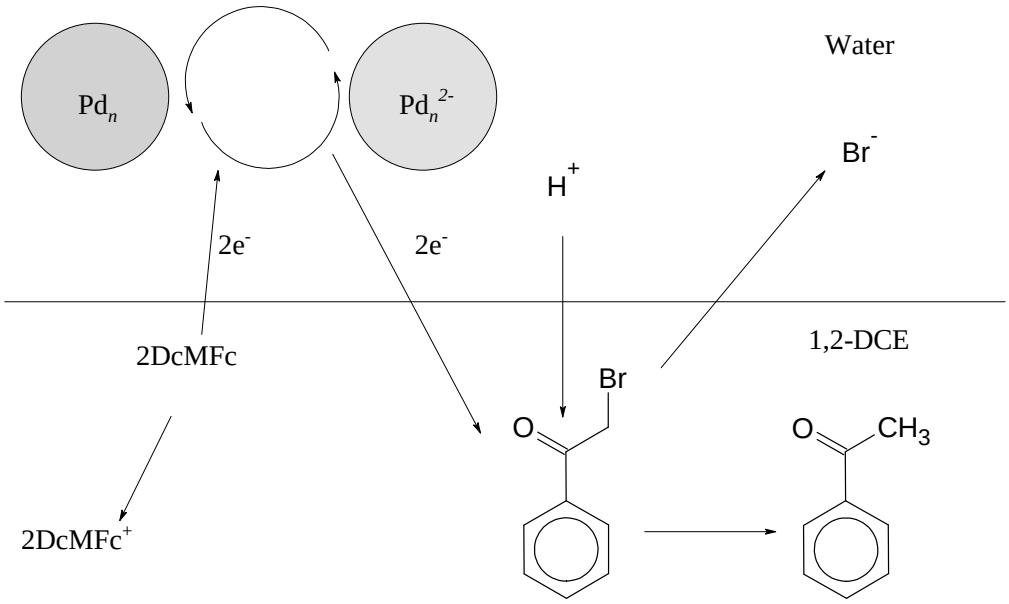

Figure 1: Schematic presentation of the dehalogenation reaction studied in publication V.

The first metal deposition study at the liquid|liquid interface was reported already in 1975 by Guainazzi *et al.* [74], where copper films were deposited at the interface. This study was also the first electron transfer study at the liquid|liquid interface. Since this work was conducted before the advent of the four-electrode potentiostat, a thorough study of the deposition reaction was not feasible. In 1996, Cheng and Schiffrin [11] reopened the subject with the electrodeposition of gold nanoparticles by reduction of $[AuCl_4]^-$(1,2-DCE) with $[Fe(CN)_6]^{4-/3-}$(aq). This system was studied by cyclic voltammetry combined with *in situ* UV-Vis spectrophotometry. The deposition reaction was reported to proceed through a three-electron transfer reaction with 20mV peak separation at higher overpotentials, but also a one-electron transfer reaction with a 60 mV peak separation at lower overpotentials. Such reversible or quasi-reversible behavior for metal deposition reactions has rarely been observed at solid electrodes. Cheng and Schiffrin [73] also deposited Pd particles at the interface by reducing $[PdCl_4]^{2-}$(aq) with decamethylferrocene(o). The driving force between these redox couples is large, and consequently, the deposition reaction proceeds spontaneously and therefore a thorough electrochemical study of the deposition process was not possible. The Pd particles were shown to possess catalytic activity in the dehalogenation of 2-bromo-acetophenone to acetophenone.

Efrima *et al.* [151–153] studied the growth of metal films and agglomerates at liquid|liquid interfaces by bringing a metal electrode tip in contact with the interface. In these studies the metal deposition occurs radially from the tip.

Publications I, II and III included in this thesis report nucleation and growth phenomena at liquid|liquid interfaces. The studies are based on the reaction between $[PdCl_4]^{2-}$(aq) and ferrocene derivatives (Fc) in the 1,2-DCE phase:

$$[PdCl_4]^{2-}(aq) + 2\,Fc(1,2\text{-DCE}) \rightarrow 2\,Fc^{+}(1,2\text{-DCE}) + 4\,Cl^{-}(aq) + Pd^{0}(s)$$

The electrochemical response for this reaction is in many aspects similar to nucleation and growth phenomena at metal electrodes, *i.e.* a current transient with an initial increase with growing nuclear size and number density, followed by a decrease invoked by the onset of linear diffusion conditions is observed. A nucleation process at a solid electrode is affected by the strong

interaction between the newly formed phase and the electrode substrate. The main difference when nucleation takes place at a liquid|liquid interface is that for the latter, this interaction is very small.

The concepts underlying nucleation at liquid|liquid interfaces are discussed in Publication I. Modeling of the nucleation and growth phenomena requires that diffusion in both phases be considered, since the charge transfer in these systems occurs by transport of electroactive species to the interfacial region from both phases. The diffusion fields thus generated are coupled and the diffusion problem in both phases must be solved. While for normal electron transfer reactions at liquid|liquid interfaces, this coupling of the diffusion fields leads to a geometrically simple model, the overlap of the multiple diffusion fields of the ensemble of nuclei in a nucleation and growth process results in a very complicated diffusion geometry. The similarities between electrodeposition at solid electrodes and at liquid|liquid interfaces inspired a generalization of a commonly used model for three-dimensional nucleation and growth at solid electrodes, based on the concept of planar diffusion fields [154–156], as described in Publication I. The concept of planar diffusion fields is further discussed in chapter 4.

Publication II considers electrodeposition of palladium under galvanostatic conditions. In this paper, a theory was formulated based on a mean concentration field. In the model, the nucleation rate law is deconvoluted from the current and potential time transients. Additionally, this model incorporates irreversible Butler-Volmer type kinetics for the growth reaction. An important experimental result resolved in the study was the observed agglomeration of particles at the liquid|liquid interface.

Publication III considers the interaction between a cluster and the surrounding liquids by a macroscopic thermodynamic approach. The theoretical conclusion of this study is that while larger particles adsorb readily at the interface, smaller particles are excluded from the interfacial region. The same theoretical approach based on interfacial and line tensions has also been used for glass beads at liquid-liquid interfaces [157] and corroborated by molecular dynamics simulations of Lennart-Jones fluids [158–160]. The electrodeposition experiments show that the thermodynamic lability of small particles can be modified by altering the interfacial tension. Correspondingly, the nucle-

ation rate constant changes. The model may be questionable in its use of macroscopic thermodynamics for microscopic systems. However, as shown in references [158–160], the use of the macroscopic quantities is accurate. The model presented in publication II was used to extract the nucleation number density transients in the absence and presence of phospholipids at the liquid|liquid interface in a potentiostatic palladium deposition experiment. This study showed that the rate constant for the growth reaction must be greater than 10^{-4} cm s^{-1}.

Recently, Platt *et al.* [76] used the reaction described in the publication I to deposit palladium particles at a γ-alumina membrane at the liquid|liquid interface. The particles were shown to grow in the pores of the membrane, and reach a maximum size determined by the pore dimensions.

In publication IV, a novel synthesis of silver particles is demonstrated. In this method, phenylpyrrole is used to facilitate the transfer of silver ions from the aqueous to the organic phase. The transferred silver ions were slowly reduced in the organic phase by pyrrole to form silver nanoparticles. A schematic of the reaction is shown in Figure 2. The detailed mechanism of the facilitated ion transfer reaction was not studied. However, the formation of the silver ion-phenylpyrrole complex serves to bring the reactants close to each other, which was assumed to be crucial for the reduction reaction and the oligomerization of the phenylpyrrole. The formation of nanoparticles was very slow, however. Assuming first order reaction kinetics, a rate constant of 0.8×10^{-3} s^{-1} was obtained by cyclic voltammetry for the consumption of the silver-phenylpyrrole complex. There is conceptual similarity with the reaction presented in chapter 5, where the reduction of palladate was carried out with thiophene-3-acetic acid in an aqueous medium.

Conjugated conducting polymers such as polyaniline, polypyrrole and polythiophenes have many potential applications including anticorrosion films, light-emitting diodes, lightweight battery electrodes, electrochromic devices, electrical contacts in semiconductors, selective membranes in biosensors and in catalysis [161–166]. Cunnane and Evans have shown that electron transfer reactions can be brought about between an aqueous-based redox system and an organic-based monomer unit (1-methylpyrrole and 1-phenylpyrrole) at an electrified liquid|liquid interface, resulting in the formation of oligomers in

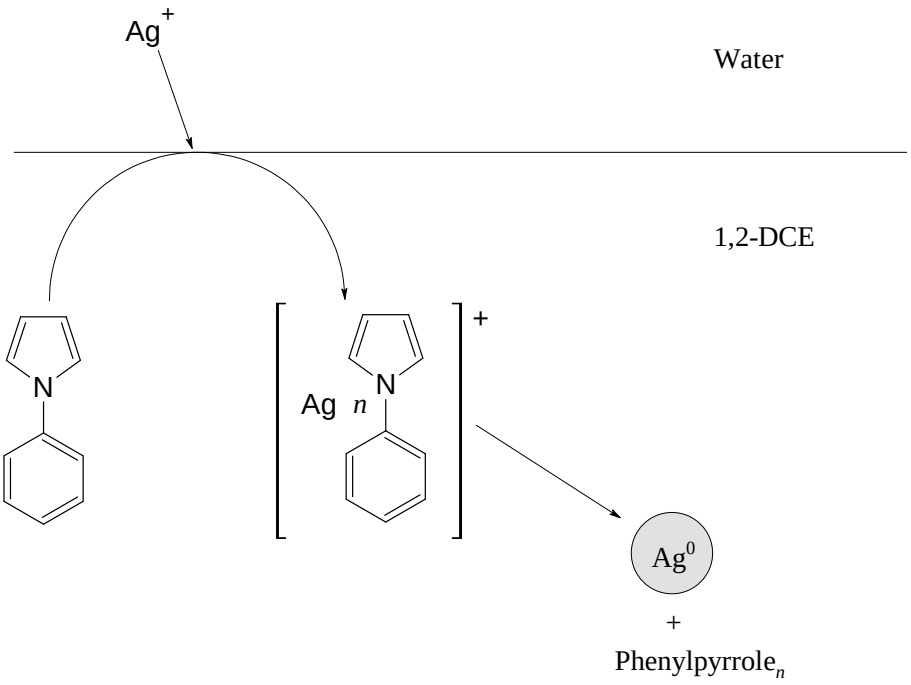

Figure 2: Schematic view of the reaction studied in publication IV.

the organic phase [75]. It was presumed that the initial electron transfer results in the formation of a radical cation in the organic phase. Later, the system was expanded to look at another electroactive monomer, 2,2':5'2" terthiophene, producing polyterthiophene [167].

Maeda *et al.* [168] demonstrated that a polymer layer can be formed at the water|1,2-dichloroethane interface by electron transfer from an adsorbed monomer to an aqueous oxidant. In this study, surface active pyrrole derivatives that adsorb at the interface from the organic phase, were used to form a Gibbs monolayer of monomers. The monolayer was polymerized by oxidation with Ce^{4+}. Additionally, it was shown that the layer formed was sufficiently compact to impede both cation and anion transfer.

4 Theories of nucleation and growth at electrodes

Electrodeposition constitutes one of the cornerstones of industrial electrochemistry. Although electrodeposition is an old, well-established technique with numerous applications, there is still a scientific interest in the technique, since it offers a unique way to study the formation of new phases through control of the supersaturation with the applied potential [11]. Accordingly, considerable attention has been given to the theory of electrochemical nucleation and growth, and the number of reports published is considerable.

In this chapter, the fundamental phenomena of nucleation kinetics are briefly presented. The emphasis is, however, on modeling of three-dimensional diffusion controlled nucleation and growth, and comparison of the models presented in this thesis to those found in the literature.

4.1 Thermodynamics and kinetics of nucleation

The initial stages of the formation and growth of new phases is of particular interest for conventional industrial electrodeposition processes, but also for the great interest in materials with nanometer dimensions [169]. The thermodynamics of small clusters deviate significantly from bulk phases due to the large fraction of surface atoms. The pioneering work on nucleation thermodynamics was reported in 1926 by Volmer and Weber [170]. The energy of a cluster can be written as a sum of its bulk and surface energies. While the former term lowers the free energy, the latter increase it. An initial energy barrier is formed for small nuclear sizes from the proportionally faster growth of the surface energy than the energy released by the formation of bulk material, see Figure 3. As the size of the cluster increases, the fraction of surface atoms, and accordingly, the significance of the surface energy term decreases. The height of the energy barrier is commonly termed the nucleation overpotential, while the cluster size at the energy maximum is termed the critical size. At the maximum, the probabilities of the cluster dissolving or growing are equal.

There have been two main approaches for quantitative evaluation of the

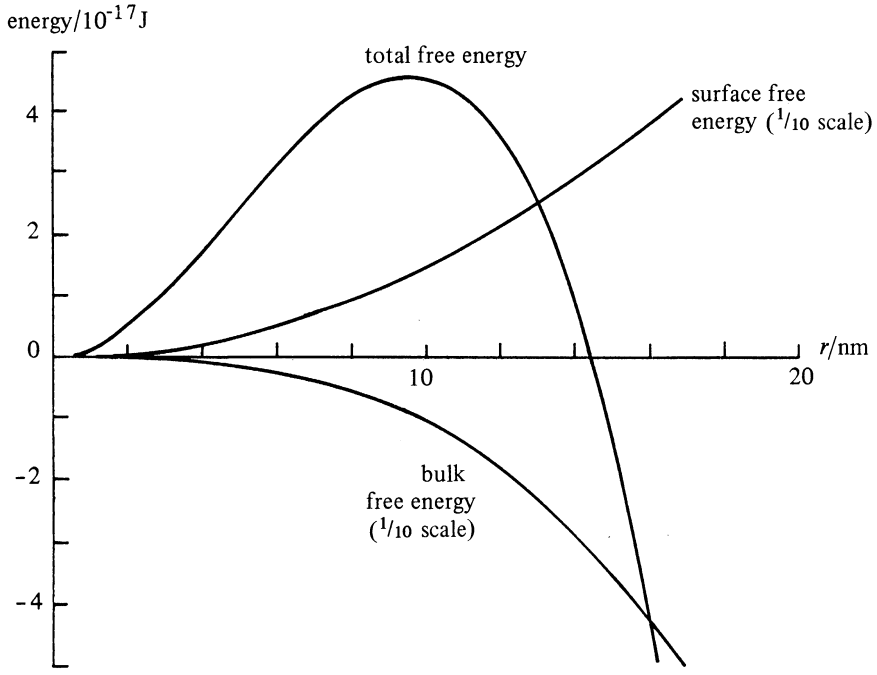

Figure 3: Free energy curves for the nucleation and growth of a spherical mercury droplet. The contributions to the total free energy made by the surface and the bulk are shown on a reduced scale [171].

nucleation rates in the literature. The classical approach [172] is based on the macroscopic surface tension concept. In this model, the size and volume of the nucleus are continuous variables. Additionally, the nucleus is assumed to be in an equilibrium form, *i.e.* the shape of the nucleus at the electrode is minimized with respect to the surface energy.

In the atomistic approach, the frequencies of attachment and detachment of atoms are defined as functions of the number of atoms in the cluster and the applied potential [172]. This approach shows that the chemical potential of a small cluster remains constant in a given supersaturation interval while the chemical potential of the parent phase changes continuously when changing the applied potential. For small clusters, the intervals are large and the use of the classical nucleation theory is not valid. With increasing cluster size, the intervals shorten and the atomistic and classical approaches coincide. Thus, this model is a discrete analogue to the classical model.

Both the classical and atomistic approach have been criticized for their inability to estimate plausible critical sizes from experimental data [173].

4.2 Diffusion controlled three-dimensional nucleation and growth

The diffusion problem in a nucleation and growth process is very complex. Generally, at short times when the nuclei and the corresponding diffusion zones are small compared to the internuclear distances, the diffusion zones surrounding the nuclei do not interact with each other, and hence, assume hemispherical shape equivalent to that of isolated nuclei. As growth proceeds, the size of the diffusion zones increase, resulting in coalescence of the diffusion zones and a gradual shift from a hemispherical to a linear diffusion regime. Thus modeling of this phenomenon is difficult since the boundary conditions that must be applied, in order to solve the concentration profiles, are very complex.

Various numerical methods have been applied to simulate the diffusion problem. Nagy and Denault [174] used Brownian dynamics to simulate instantaneous nucleation and growth, following a large potential step, at hexagonal and square arrays. Fransaer and Penner [169] studied instantaneous

nucleation and growth by Brownian dynamics with a spatially random distribution of nuclei. The attention was focused on the evolution of particle size dispersion as a function of the experimental variables. It was found that the particle size distribution initially converges, but with the onset of overlap of the diffusion fields, the particle size distribution diverges. They concluded that size dispersion is caused by an inhomogeneous distribution of interparticle distances which translates into an inhomogeneity in the diffusion-limited flux at each particle. Brownian dynamics simulations are, even on fast modern computers, time consuming due to the large system that must be considered. The accuracy of such simulations suffers from the limited number of nuclei and metal ions, *i.e.* the volume of the solution. Cao *et al.* [175] used a boundary integral method to simulate both instantaneous and progressive nucleation. Their simulations do not suffer from the limitations mentioned above as the number of nuclei exceeded 5000, and additionally, the simulations were extended sufficiently far into the bulk solution. Hence, these simulations should reproduce the real concentration profiles and fluxes accurately.

Most theoretical approaches consider first the growth of a single nucleus, and then approximate the overlap of diffusion fields to obtain the current to multiple nuclei. The case of an isolated nucleus is easy to solve in a quasi-stationary approximation, where the diffusion field is assumed to develop much faster than the nucleus grows. The resulting equations for a hemisphere growing at a solid electrode are

$$R(t) = \left(2Dc^{\mathrm{b}}\bar{V}t\right)^{1/2} \tag{6}$$

and,

$$i(t) = \pi z F \bar{V}^{1/2} (c^{\mathrm{b}} D)^{3/2} t^{1/2} \tag{7}$$

where $i(t)$ is the current to the nucleus, $R(t)$ is the radius of the nucleus, z is the charge transferred, F is Faraday's constant, $\bar{V}$ is the molar volume of the deposited phase, D is the diffusion coefficient and c^{b} is the bulk concentration of the reacting species. This problem can also be solved exactly [176], however, the resulting expressions are complicated, and additionally, the numerical error resulting from the quasi-stationary assumption is negligible for

common values.

Sharifker *et al.* [154–156] introduced the concept of planar diffusion zones to approximate the effect of merging diffusion fields on the observed current density to a planar electrode. In this approach, the hemispherical diffusion zone surrounding an isolated nucleus is mapped into a hypothetical planar zone of circular shape, to which only linear diffusion perpendicular to the electrode surface is allowed. The radius of the diffusion zone is solved by equating the fluxes for the hemispherical and planar diffusion fields. The first assumption in this model is that for a distribution of nuclei with interacting diffusion fields, the solution of the real diffusion problem can be approximated by the flux to the area fraction covered by diffusion zones. The current transient to the ensemble of nuclei is obtained by multiplying the covered area fraction with the Cottrell equation initiated at the beginning of the potential step, where the area fraction covered with randomly distributed circles is calculated by the Avrami theorem [177]. This is the second assumption in this model. Thus, the current to any nucleus on the electrode, *i.e.* diffusion zone, independently of the time of formation, is given by the Cottrell equation, initiated at the beginning of the potential step.

Several attempts have been made to improve this model. Sluyters-Rehbach *et al.* [178] argued that in order to preserve a uniform thickness of the diffusion layer appropriate to planar diffusion, the hypothetical planar flux should not relate only to their age but also to their time of formation. In the model by Mirkin and Nilov [179], it was noted that multiplying the covered area fraction with the Cottrell equation is not correct as the planar diffusion zones in progressive nucleation have different times of formation, and hence, must be accounted for by initiating the Cottrell equation at different times for each zone. Heerman *et al.* [180–182] have later presented the same theory as Mirkin and Nilov, and discussed the resulting transients in detail. For instantaneous nucleation, all models reduce to the same expression for the current-time transient.

These models all yield similar results, the main difference being only in the way the current to the diffusion zones is calculated, and accordingly, parameters extracted from experimental data are similar. Numerical simulations [169,174,175] show that the established analytical expressions quite ad-

equately reproduce the instantaneous current time transients resulting from a potential step, despite the coarse approximations that have been made to obtain an analytical solution.

4.3 Evaluation of the models presented in this thesis

One aim of publication I (model I) was to generalize the concepts of nucleation for liquid|liquid interfaces. The details specifically regarding the liquid|liquid interface are discussed in section 3.5. The definition of planar diffusion zones was also reconsidered in publication I, in that the growth of the diffusion zones was accounted for by initiating linear flux conditions continuously as the fraction covered by the planar diffusion zones expands. This was motivated by the fact that applying the Cottrell equation directly to a moving boundary problem is incorrect. Thus, in this model the thickness of the diffusion layer, and hence the flux density, depends on the time of coverage of the point considered. This model also relies on the postulate that the real diffusion and growth problem can be approximated by its two-dimensional projection, *i.e.* the concept of planar diffusion zones.

Publication II deals with galvanostatic nucleation and presents an alternative approximation for the diffusion problem. While the models based on planar diffusion zones reproduce experimental transients following potential steps to a satisfactory level, the physical foundation of the concept is controversial. There is no evident justification for why overlap in nucleation can be evaluated by the overlap of the two-dimensional mapping of the three-dimensional real diffusion fields, and consequently, this concept is difficult to generalize for variable potential functions and growth kinetics. Hence, a different model was needed for this type of problem.

In the model presented in Publication II (model II), the spherical diffusion field surrounding each particle is retained. However, the bulk concentration is replaced with the average interfacial concentration at the electrode. This approximation divides the diffusional flux into two contributions, one linear for the ensemble and one hemispherical specific to the nuclei under consideration and is motivated by the fact that the spherical diffusion geometry is located close to the nucleus, and thus, the error introduced by using the average interfacial concentration as an effective bulk concentration is small.

The average interfacial concentration can be easily calculated by convolution of the current obtained experimentally. The growth rate of the particle is dependent both on the time of formation and the history of the experiment, which is reflected in the time dependence of the average interfacial concentration. The use of a hemispherical geometry allows the use of simple and familiar equations. However, solving the current transient for a predefined potential function and nucleation rate law, requires the solution of integral equations and is therefore somewhat more tedious.

In order to evaluate models I and II, the resulting current transients for instantaneous nucleation following a large potential step, where the surface concentration at the nucleus can be considered to equal zero, are compared to the simulations made by Cao *et al.* [175] and the Scharifker model [154–156]. The models by Sluyters-Rehbach *et al.* [178], Mirkin and Nilov [179], and Heerman *et al.* [180–182] reduce to the Scharifker model for instantaneous nucleation and are therefore not considered separately. The following parameters were used: $D = 0.71 \times 10^{-5}$ cm^{2}s^{-1}, $N_0 = 1.0 \times 10^8$ cm^{-2}, $n = 1$ and $\overline{V}$=7.14 cm^{3}mol^{-1}. c^{b} ranged from 1.0 to 100 mM. These values were used in the simulations made by Cao *et al.* and are typical for deposition of copper from acidic solutions [175]. The calculated current transients are based on the equations presented in Publication I, II, and reference [154].

Model I gives the following expression for instantaneous nucleation at solid electrodes

$$j(t) = 2zFc^{\mathrm{b}}(\alpha D N_0)^{1/2}\Phi\left((\pi\alpha N_0 t)^{1/2}\right) \tag{8}$$

where Φ is Dawson's integral and α is given by:

$$\alpha = D\left(2\pi\bar{V}c^{\mathrm{b}}\right)^{1/2} \tag{9}$$

In publication I, the expression for α was incorrectly given for the case of hemispherical particles growing on a solid electrode, however, it was correct for liquid|liquid interfaces which was the focus of the paper.

The current transients for model II were calculated from eqns. 3, 6 and 10 in publication II with the conditions outlined above, *i.e.* $\Delta c(t) = c^{\sigma}(t)$ and $N(t) = N_0$ for $t \geq 0$. All integrations were performed by the trapezoidal

rule. The transients of the Scharifker model were calculated from equations (12) and (15) given in reference [154].

The resulting transients are shown in Figure 4 for a) 100 and b) 1 mM. All transients have been reduced by the peak current and peak time given by the Scharifker model. Typically, the peak occurs at *ca.* 1-10 s, depending on the nuclear number density used.

In comparison to the simulations by Cao *et al.*, model I overestimates the peak current by 10-20% depending on the concentration. Model II overestimates the peak current by only 0.5-3.8% with the error decreasing with increasing concentration. The Scharifker model overestimates the peak current by 3.7% at 1 mM and underestimates the peak current by 3% at 100 mM.

Although the Scharifker model describes the current transient well, it is inconsistent in that the concentration profile above any point of the electrode, regardless of whether the considered point is located inside a diffusion zone or not, is assumed to be equivalent to that corresponding to linear diffusion conditions initiated at $t = 0$. As a consequence, the current obtained using the Scharifker model is always smaller than or equal to that given by the Cottrell equation, which does not correspond to the simulation findings, especially at longer time scales. However, the error is generally small (-7.3% at five peak times).

In model I, a fully developed diffusion profile outside the diffusion zones is not assumed, and hence, the current is not limited below the Cottrell transient. However, quantitatively the performance of model I is clearly inferior to the other models. As discussed in publication I, the model is inconsistent in that the predicted current transients depend on the species under consideration, which violates the mass balance at the interface. This problem is inherent to all models that are based on planar diffusion zones.

Model II reproduces the simulated current transient and all of its qualitative features well. Thus, the approximation of the diffusion problem used in publication II appears to be valid, particularly at higher concentrations and lower nuclear densities when the hemispherical diffusion field is small compared to the internuclear distances.

In conclusion, for potentiostatic experiments, where the above conditions

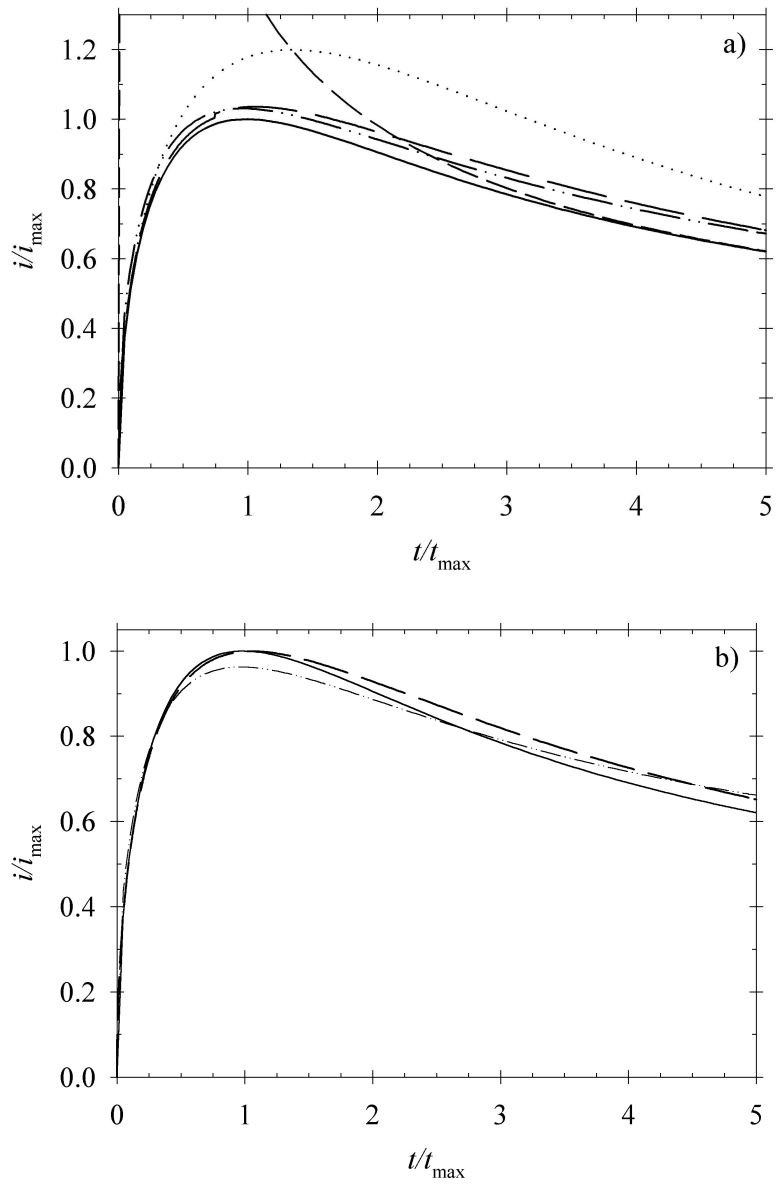

Figure 4: Current time transients calculated for instantaneous nucleation. a) Transients calculated for c^{b}=100 mM. (– – –) Cottrell transient, (——) Scharifker model, ($\cdots$) Model I, (— —) Model II, and (— ·· —) simulated current [175]. b) Transients calculated for c^{b}=100 mM. (——) Scharifker model, (— —) Model II, and (— ·· —) simulated current [175]. The following parameters were used: $D = 0.71 \times 10^{-5}$ cm^{2}s^{-1}, $N_0 = 1.0 \times 10^8$ cm^{-2}, $n = 1$ and V=7.14 cm^3 mol^{-1}.

Table 1: Comparison of the nucleation models. Errors are calculated with the parameters given in the text and $c^{\mathrm{b}} = 100 \times 10^{-6}$ mol cm^{-3}.

	Scharifker Model	Model I	Model II
Basis	Planar diffusion zones	Planar diffusion zones	Mean concentration
Error at 1×peak time	-3.0%	16.4%	0.5%
Error at 5×peak time	-7.3%	16.2%	1.9%
Performance	Good	Poor	Good
Ease of use	Easy	Easy	Intermediate

are fulfilled, model II and the Scharifker model perform equally well with respect to the experimental errors encountered in nucleation experiments. In this case, the Scharifker model provides a computationally facile and appealing alternative, that yields accurate results. However, for more complicated experimental systems, *e.g.* liquid|liquid interfaces, a consistent approach must be taken that reflects the true diffusion profiles, and for this purpose, model II is clearly better than the other models. The boundary integral method used by Cao *et al.* [175] should be considered, if the computational effort can be afforded. The performance of the models is summarized in Table 1.

5 Synthesis of palladium nanoparticles from palladate and thiophene in aqueous media

This chapter describes a previously unpublished synthesis of palladium nanoparticles, by the reduction of palladate with thiophene-3-acetic acid. The particles were characterized by WAXS, SAXS, XPS, UV-Vis and TEM. A particle size range of 1-4 nm was found. The acidic group on the particles features pH tunable aqueous solubility.

5.1 Introduction

There has recently been a growing interest in composites of metal nanoparticles and conducting polymers. These materials show various interesting features, particularly, energy storage, catalytic activity, magnetic susceptibility, and unique dielectric properties [183]. Electrodes can also be modified with nanoparticle-conducting polymer composites [184–186]. Such electrodes are of interest in catalysis and electroanalytical applications.

Tamil Selvan *et al.* [187–190] presented a novel synthesis of conducting polymer encapsulated gold nanoparticles, using pyrrole as the electron donor for the reduction of $[AuCl_4]^-$, to yield 7 nm gold nanoparticles in pyridine block copolymers. Upon oxidation, the pyrrole monomer polymerizes to form a protective layer around the particle. Zhou *et al.* [191] have shown that a conjugated polymer, poly(dithiafulvene), can be used to reduce noble metal ions (Au, Pd and Pt) to form nanoparticles protected by the polymer. Recently, we demonstrated that silver particles can be generated at electrified liquid|liquid interfaces, see publication IV. In this reaction, aqueous silver ions transfer to the 1,2-dichloroethane phase, and react with phenylpyrrole to form metallic particles. The ion transfer reaction is facilitated by complex formation with phenylpyrrole.

This chapter presents the synthesis and characterization of metallic palladium nanoparticles, formed by reduction of palladate with thiophene-3-acetic acid. In the considered reaction, thiophene-3-acetic acid forms a stabilizing layer protecting the particle. The solubility properties of the particles can be adjusted by altering the pH of the aqueous medium. An evident question

is the possible polymerization of the thiophene-3-acetic acid.

5.2 Experimental

In a typical synthesis, Pd nanoparticles were prepared by mixing 50 ml of 20 mM thiophene-3-acetic acid (TCI) in 50 mM H_2SO_4(aq) (Merck) and 50 ml of 4 mM $(NH_4)_2PdCl_4$ (Alfa Aesar) in 50 mM H_2SO_4(aq) at room temperature under a nitrogen atmosphere. Upon mixing the two solutions, a black precipitate formed indicating that a reaction between thiophene-3-acetic acid and palladate had taken place. The precipitate was washed several times with water and dried under vacuum. This particular precipitate is later referred to as **a**. The precipitate was dissolved in 0.1M NaOH(aq) (Merck) to yield a black colloidal solution, later referred to as **b**.

Wide angle X-ray scattering (WAXS) measurements were performed using a Siemens $\theta - 2\theta$ diffractometer with Cu K_α (1.542) radiation monochromatized with a nickel filter in the incident beam and a totally reflecting glass surface. The scattered intensities were measured with a Hi Star area detector and an angular range of 2θ=17-47°, an angular step of 0.1°, and a measurement time of 60 s per point.

Small angle X-ray scattering (SAXS) measurements were done with a sealed fine-focus Cu K_α tube mounted in the point-focus position. The beam was monochromatized with a nickel filter and totally reflecting glass surface (Huber 701 small-angle chamber). The data were measured with a one-dimensional position sensitive proportional counter (MBraun OED- 50M). A wave-vector range of 0.02-0.45 $Å^{-1}$ was covered.

The particles were examined using a JEOL 2010 transmission electron microscope (TEM), operating at 210 keV. Standard preparative methods were used to disperse the particles from **b** onto a lacy carbon TEM grid. Several different regions of the TEM specimen were examined.

High resolution X-ray photoelectron spectroscopy (XPS) measurements were carried out on an AXIS 165 (KRATOS Analytical) photoelectronspectrometer, with charge compensation by thermal electrons. Energy levels ranging from 0 to 1100 eV were recorded. High resolution (HiRes) measurements were carried out for C 1s, O 1s, Pd 3p and S 2p with an energy resolution of 0.1 eV. The samples were prepared by placing precipitate (**a**)

on a piece of filter paper. The spectra were recorded at six different spatial locations. The C 1s core level of the C-C bond was used as an internal standard (285.0 eV [192]). Oxygen was determined from the Auger O(KLL), since the Pd 3p core level interferes with the O 1s level. The contributions from the filter paper (C and O) were subtracted from the results.

The UV-Vis spectra were recorded on a Hewlett Packard HP8451A diode array spectrophotometer in a 1 cm light path length quartz cuvette from a dilute solution of **b**.

5.3 Results

As shown below, precipitate **a** contained small particles of 1-4 nm size. The particles can be repeatedly precipitated and redispersed with HCl and NaOH without any changes in appearance. Such property can be explained only by the functionalization of the particle surface with acid groups, and may be considered as evidence of the presence of the acid group of the thiophene moiety. The thiophene-3-acetic acid is discussed below.

The WAXS pattern of **a** is shown in Figure 5. The diffraction pattern included the 111 reflection of palladium, showing that the particles are metallic. The size of the crystallites, as calculated from the Scherrer formula, was approximately 1.5 nm. It is noted here that the accuracy of the Scherrer equation is insufficient for particles in this size range, and this value should be taken only as indicative. The WAXS pattern of thiophene-3-acetic acid is also shown in Figure 5.

The size distribution obtained from SAXS, along with the experimental and modelled intensities (inset), are presented in Figure 6. The particle size distribution was modelled as a polydisperse system of spherical Pd particles in a matrix [193]. The volume distribution was assumed to be bimodal consisting of two gaussian functions. The SAXS data suggests a narrow size distribution, with a mean particle size of 2.2 nm and standard deviation of 1.0 nm. The distribution could be well described by a single gaussian, indicating that the choice of the bimodal distribution describes the size distribution satisfactorily. This size range is comparable to that calculated from the WAXS data.

TEM was employed to obtain information about the morphology of the

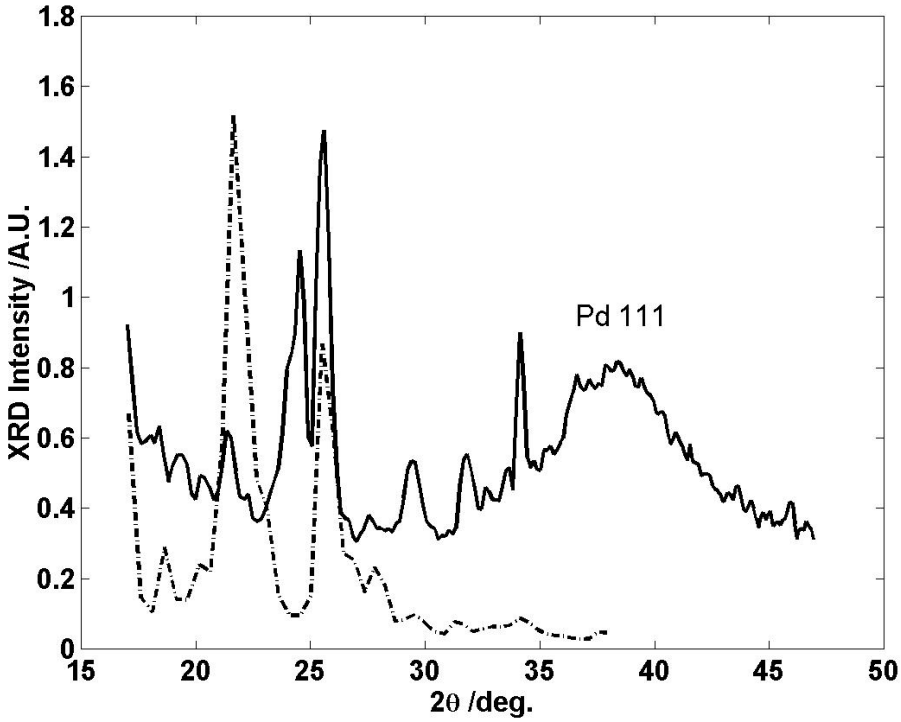

Figure 5: The WAXS pattern of **a** (——) and thiophene-3-acetic acid (– · –).

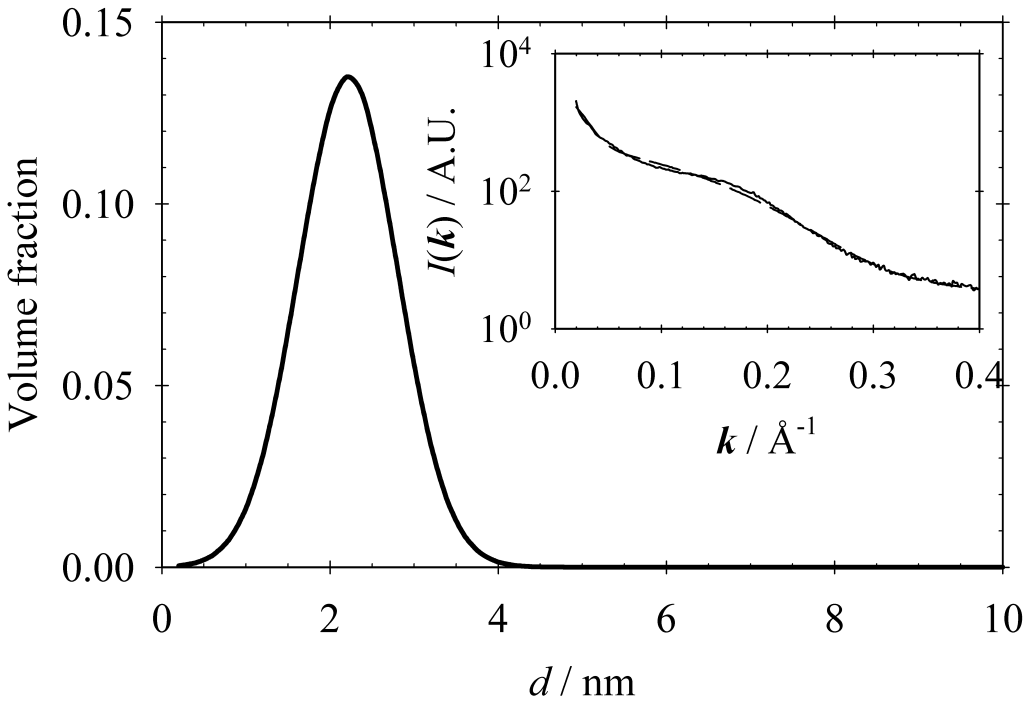

Figure 6: The volume distribution of spherical particles fitted to the SAXS data. The experimental (——) and model intensities (— —) are shown in the inset.

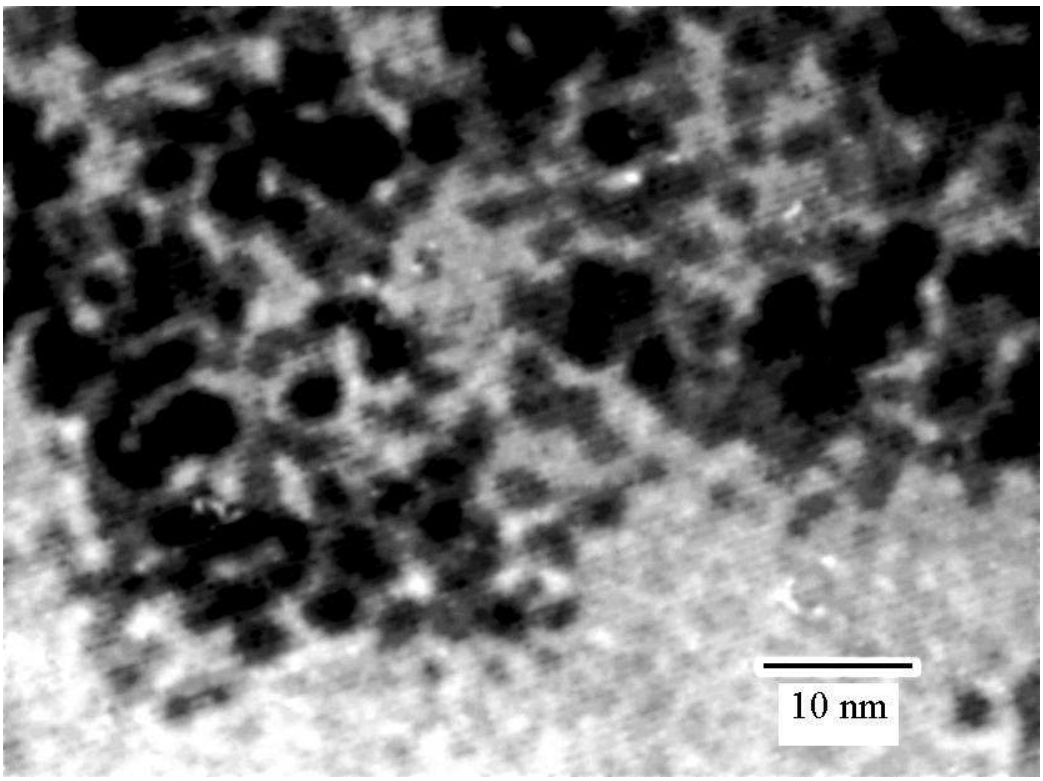

Figure 7: TEM photograph of the particles. The bar in the lower right corner corresponds to 10 nm. Estimated average particle size is 2-3 nm.

particles. A typical TEM image of the particles dispersed on a carbon support is shown in Figure 7. Aggregates of near spherical particles can be seen. The size distribution was not calculated due to the poor quality of the TEM photograph. However, some particles can be clearly distinguished. These are in the 2-3 nm size range, which compares favorably to the size distribution calculated from the SAXS data.

The chemical composition and the oxidation states of the elements in **a** were investigated with XPS. In the XPS spectrum, see Figure 8 a, a doublet of Pd $3d^{5/2}$ at 336.2eV with two narrow peaks is further evidence that palladium is present in its metallic state. This also corresponds to that found for a vapor deposited palladium metal standard obtained with the same equipment. No other oxidation states of palladium were detected in the sample. A narrow S $2p^{1/2}$ peak was found at 164.2 eV, see Figure 8 b, which corresponds favorably with that reported for thiophene, 164.3 eV [194]. Sulfur could not

be detected in any other chemical environment than that of thiophene. The Pd/S ratio calculated from the XPS intensities was 3.1. This corresponds to approximately one thiophene group for every 1.6 surface atoms in a 2.2 nm particle. For a densely packed structure, the majority of thiophene groups can be directly adsorbed at the metal surface. The metallic state can also be seen as a Fermi level extending through 0 eV, a feature that is unique for conductive materials, see Figure 8 c.

The UV-Vis spectra of thiophene-3-acetic acid, and **b** are shown in Figure 9. The spectrum of **b** agrees well with that calculated by Creighton *et al.* [195] for the surface plasmon of 10 nm Pd particles, however with two peaks (2 and 3) at 218 and 242 nm. It is noted here that absorption spectra of metal particles between 3-20 nm are only weakly dependent on particle size [195]. The size range found in this study is at the lower limit of this range, and therefore conclusions should be taken only as indicative. The spectrum of **b** shows a shoulder at 340-400 nm. These wavelengths correspond to the absorption of poly(thiophene-3-acetic acid) [196, 197], and may thus be an indication of the formation of poly(thiophene-3-acetic acid). Unfortunately, a corresponding absorption band would be masked by the absorption of the colloid, and therefore, difficult to resolve. The possible formation of oligomers is discussed later on. For comparison, the UV-Vis spectrum of thiophene-3-acetic acid is also shown. The thiophene-3-acetic acid has a peak at 208 nm (Peak (1)). This peak is not present in the colloid, indicating that thiophene-3-acetic acid is not present at significant concentrations in its free form. The possible relation between peak (1), (2) and (3) was not resolved in this study, however, shifts towards longer wavelengths may relate to a higher conjugation of π-orbitals.

5.4 Discussion

The mechanism of the reaction between palladate and thiophene-3-acetic acid is of considerable importance for the resulting products, especially regarding thiophene-3-acetic acid. As shown above, the metallic nature of the particles is apparent. Thus, a redox reaction, involving electron transfer from the thiophene-3-acetic acid to the Pd^{2+} center, must have taken place. The thiophene ring is known to act as an electron donor, and under suit-

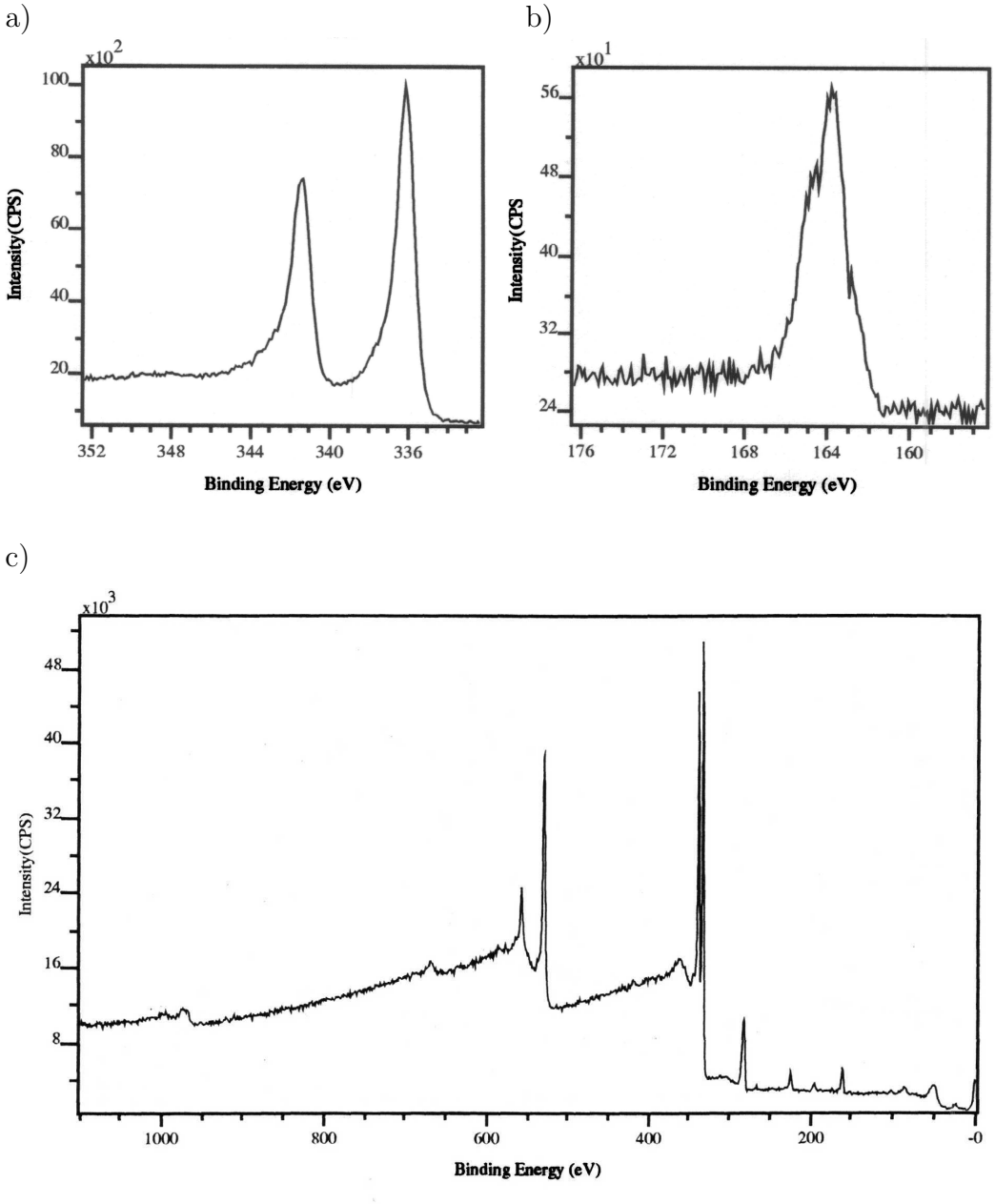

Figure 8: XPS spectra of **a**. a) Pd $3d^{5/2}$ b) S $2p^{1/2}$, and c) wide spectrum.

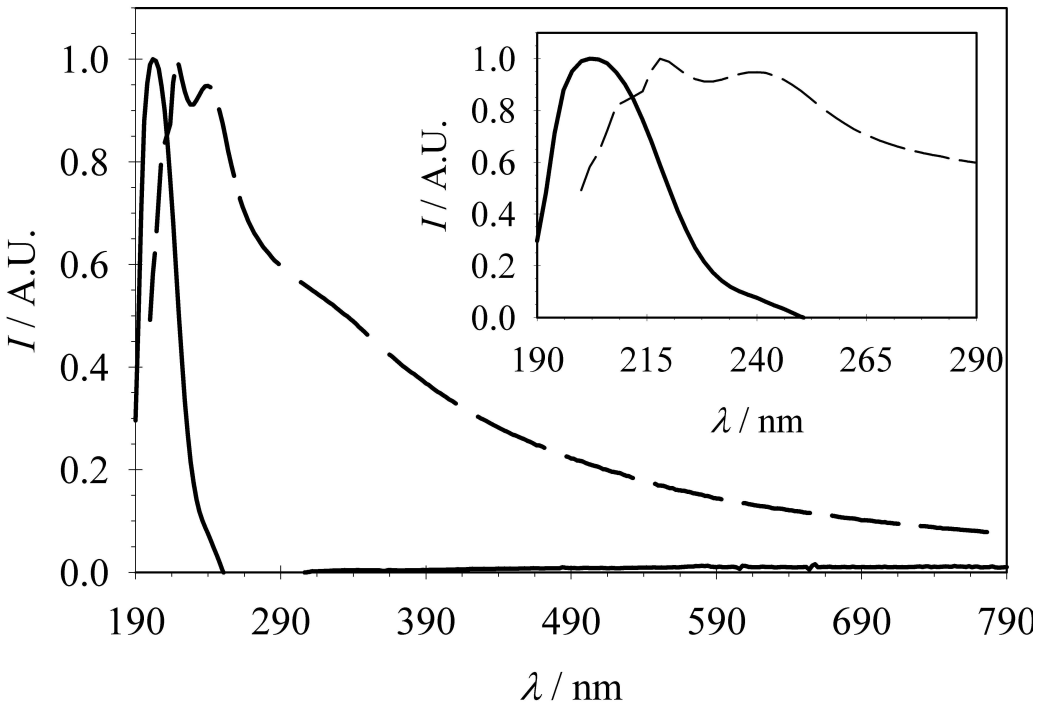

Figure 9: UV-Vis absorption spectra of thiophene-3-acetic acid (——) and compound **b** (— —).

able conditions oxidation of the thiophene results in proton loss followed by polymerization, where the polymerization step is believed to proceed through radical-radical or radical-monomer coupling [198]. Proton loss followed by coupling of the monomers results in a lower reaction free energy, and is thus energetically more favorable than simple monomer oxidation. Generally, electropolymerization of thiophene is carried out in non-aqueous solutions. However, thiophene have been shown to polymerize at Pt electrodes from aqueous solutions, where it has been solubilized by surfactants, to overcome the low aqueous solubility [199].

In this study, a shoulder was found in the UV-Vis spectrum at the wavelengths corresponding to poly(thiophene-3-acetic acid), *i.e.* 340-400 nm, and also the absorption peak of thiophene-3-acetic acid has been shifted to longer wavelengths. The XPS spectra shows that the thiophene ring is present at the particle surface and that sulfur is present only in thiophene. A possible reaction mechanism involves the formation of a precursor complex, which by bringing the thiophene moieties close together favors polymerization. The evidence supporting polymerization in this study is not conclusive, and thus, other reaction mechanisms also should be considered.

5.5 Conclusions

In conclusion, the formation of nanoparticles in the 1-4 nm size range has been observed by both TEM, WAXS and SAXS. The metallic nature of these particles has been confirmed by both XPS and WAXS. The UV-Vis spectrum of the colloid also indicates the formation of Pd^0 nanoparticles. The pH dependent solubility properties of these particles is a clear indication that the carboxylic acid group is present on the particles.

These particles have interesting properties, *e.g.* the pH tuneable ion-exchange membrane surrounding the particles may prove useful in catalysis and electrocatalysis, *e.g.* immobilized on polythiophene coated electrodes. Additionally, the particles could, *in principle*, be precipitated in size fractions by varying the pH.

Further work on the characterization of these particles is still required. In particular, infrared spectroscopy, solid state NMR and mass spectroscopy should be attempted to resolve the question of polymerization.

6 Conclusions

The aim of this thesis was to study the formation, growth and properties of metal nanoparticles. Special emphasis was placed on reactivity and formation of such particles at liquid|liquid interfaces. Based on the results obtained in this work, the following conclusions can be drawn:

The electrodeposition studies presented in publications I-III show that the electrified liquid|liquid interface is suitable to study the initial steps of nucleation, with the advantage of controlling the growth reaction with the applied potential, while not suffering from the presence of strong interactions between the electrode and the new phase. In publication I, a novel model based on the concept of planar diffusion fields was presented. It was shown that this approach is inconsistent and therefore, not generally applicable to the liquid|liquid interface, since the overlap and hence current are dependent on the species under consideration.

In publication II, a new model based on average interfacial concentrations was developed. This model overcomes the problems encountered in the first publication. Additionally, it was shown that the mean interfacial concentration can be used as a good approximation for the overlap of the diffusion zones. The interpretation of the experimental results indicates that the particles formed at the interface agglomerate.

In publication III, the adsorption of particles at liquid|liquid was considered. A thermodynamic model was developed based on macroscopic surface and line tensions. It was shown in the experimental work that the addition of phospholipids destabilizes the embryonic clusters at the initial stages of growth, and thereby, decreases the nucleation rate.

Publication IV demonstrates how the liquid|liquid interface can be used to study the formation of nanoparticles in a homogeneous phase. In the study, silver ions were transferred by facilitated ion transfer from the aqueous to the organic phase where their reduction and agglomeration to form particles occurs. 1-Phenylpyrrole functions both as the complexation agent in the facilitated ion transfer reaction and as the reductant in the electron transfer reaction. The oxidation of 1-phenylpyrrole was believed to result in poly(phenylpyrrole). The reaction rate was noted to be too slow for practical

purposes.

In chapter V, the reaction between palladate and thiophene-3-acetic acid resulting in 1-4 nm sized nanoparticles was discussed. The nanoparticles were characterized by TEM, XPS, WAXS, SAXS and UV-Vis. These particles were soluble in aqueous solutions, with pH-tunable solubility properties. Although no direct evidence was obtained, the oxidation of thiophene-3-acetic is believed to result in oligomerization.

Publication V demonstrates the use of a colloidal aqueous phase for the two-phase electrocatalytic dehalogenation of 2-bromoacetophenone. Additionally, it was shown by cyclic voltammetry and electrophoretic light scattering measurements that the aqueous colloids can be charged with electrons by a two-phase process involving decamethylferrocene as the electron donor.

References

[1] K. E. Drexler, Nanosystems: molecular machinery, manufacturing, and computation, Wiley Interscience, London, 1992.

[2] A. Henglein, *Chem. Rev.* **89** (1989) 1861.

[3] G. Schmid, *Chem. Rev.* **92** (1992) 1709.

[4] C. N. R. Rao, G. U. Kulkarni, P. J. Thomas, P. P. Edwards, *Chem. Soc. Rev.* **29** (2000) 27.

[5] A. C. Templeton, W. P. Wuelfing, R. W. Murray, *Acc. Chem. Res.* **33** (2000) 27.

[6] G. Markovich, P. Collier, S. E. Henrichs, F. Remacle, R. D. Levine, J. R. Heath, *Acc. Chem. Res.* **32** (1999) 415.

[7] L. N. Lewis, *Chem. Rev.* **93** (1993) 2693.

[8] R. Elghanian, J. J. Storhoff, R. C. Mucic, R. L. Letsinger, C. A. Mirkin, *Science* **277** (1997) 1078.

[9] D. I. Gittins, D. Bethell, D. J. Schiffrin, R. J. Nichols, *Nature* **408** (2000) 67.

[10] S. W. Koch, A. Knorr, *Science* **293** (2001) 2217.

[11] Y. F. Cheng, D. J. Schiffrin, *J. Chem. Soc., -Faraday Trans* **92** (1996) 3865.

[12] J. A. Mellor, A comprehensive treatise on inorganic and theoretical chemistry, Longmans, Green & Co, London, 1923.

[13] M. Faraday, *Philos. Trans. Soc. London* **197** (1857) 145.

[14] G. Schön, U. Simon, *Colloid Polym. Sci* **273** (1995) 101.

[15] G. Schmid, M. Bäumle, M. Geerkens, I. Heim, C. Osemann, T. Sawitowski, *Chem. Soc. Rev.* **28** (1999) 179.

[16] G. Schmid, R. Ugo (Ed.), Vol. 7 of *Aspects of homogeneous catalysis*, Kluwer Academic Press, 1991, pp. 1–36.

[17] P.-A. Buffat, M. Flüeli, P. Stadelmann, J.-P. Borel, *Faraday Discuss. Chem. Soc.* **92** (1991) 173.

[18] J. H. Fendler (Ed.), Nanoparticles and nanostructured Films: Preparation, Characterization and Applications, Wiley-VCH, 1998.

[19] Y. Wang, J. Ren, K. Deng, L. Gui, Y. Tang, *Chem. Mater.* **12** (2000) 1622.

[20] R. W. Devenish, T. Goulding, B. T. Heaton, R. Whyman, *J. Chem. Soc., -Dalton Trans.* (1996) 673.

[21] J. R. Thomas, *J. Appl. Phys.* **37** (1966) 2914.

[22] C. H. Griffiths, H. P. O'Horo, T. W. Smith, *J. Appl. Phys.* **50** (1979) 7108.

[23] T. Tano, K. Esumi, K. Meguro, *J. Colloid Int. Sci.* **133** (1989) 530.

[24] T. Tano, K. Esumi, K. Meguro, *Colloid Surf.* **62** (1992) 255.

[25] N. Arul Dhas, H. Cohen, A. Gedanken, *J. Phys. Chem. B* **101** (1997) 6834.

[26] N. Arul Dhas, A. Gedanken, *J. Mater. Chem.* **8** (1998) 445.

[27] A. Henglein, *J. Phys. Chem.* **97** (1993) 5457.

[28] M. T. Reetz, W. Helbig, *J. Am. Chem. Soc.* **116** (1994) 7401.

[29] M. T. Reetz, S. A. Quaiser, *Angew. Chem. Int. Edit.* **34** (1995) 2240.

[30] M. T. Reetz, M. Winter, R. Breinbauer, T. Thurn-Albrecht, W. Vogel, *Chem.-Eur. J.* **7** (2001) 1084.

[31] H. Bönnemann, W. Brijoux, R. Brinkmann, R. Fretzen, T. Joussen, R. Köppler, B. Korall, P. Neiteler, J. Richter, *J. Mol. Catal.* **86** (1994) 129.

[32] J. Turkevich, G. Kim, *J. Macromol. Sci. -Chem.* **169** (1970) 873.

[33] H. Hirai, Y. Nakao, N. Toshima, *J. Macromol. Sci. -Chem.* **A13** (1979) 727.

[34] M. Komiyama, H. Hirai, *Bull. Chem. Soc. Jpn.* **56** (1983) 2833.

[35] H. Hirai, Y. Nakao, N. Toshima, *J. Macromol. Sci. -Chem.* **A13** (1979) 633.

[36] W. Hoogsteen, L. G. J. Fokkink, *J. Coll. Int. Sci.* **175** (1995) 12.

[37] L. D. Rampino, F. F. Nord, *J. Am. Chem. Soc.* **63** (1941) 2745.

[38] A. Henglein, M. Giersig, *J. Phys. Chem. B.* **103** (1999) 9533.

[39] H. Bönnemann, R. Brinkmann, R. Köppler, P. Neiteler, J. Richter, *Adv. Mater.* **4** (1992) 804.

[40] C. Petit, P. Lixon, M. P. Pileni, *J. Phys. Chem.* **9** (1993) 12974.

[41] A. Taleb, C. Petit, M. P. Pileni, *Chem. Mater.* **9** (1997) 950.

[42] M. Brust, M. Walker, D. Bethell, D. J. Schiffrin, R. Whyman, *J. Chem. Soc. -Chem. Commun.* (1994) 801.

[43] M. Brust, J. Fink, D. Bethell, D. J. Schiffrin, C. Kiely, *J. Chem. Soc. -Chem. Commun* (1995) 1655.

[44] M. Brust, D. Bethell, D. J. Schiffrin, C. J. Kiely, *Adv. Mater.* **7** (1995) 795.

[45] S. Chen, R. S. Ingram, M. J. Hoestetler, J. J. Pietron, R. W. Murray, T. G. Schaaff, J. T. Khoury, M. M. Alvarez, R. L. Whetten, *Science* **280** (1998) 2098.

[46] W. L. Wilson, P. F. Szajowski, L. E. Brus, *Science* **262** (1993) 1242.

[47] C. B. Murray, D. J. Noris, M. G. Bawendi, *J. Am. Chem. Soc* **115** (1993) 8706.

[48] T. G. Schaaff, M. N. Shafigullin, J. T. Khoury, I. Vezmar, R. L. Whetten, W. G. Cullen, P. N. First, C. Gutierrez-Wing, J. Ascensio, M. J. Jose-Yacaman, *J. Phys. Chem. B* **101** (1997) 7885.

[49] W. Nernst, E. Riesenfeld, *Ann. Phys* **8** (1902) 600.

[50] F. M. Karpfen, J. E. B. Randles, *Trans. Faraday Soc.* **49** (1953) 823.

[51] C. Gavach, T. Mlodnicka, J. Guastalla, *C. R. Acad. Sci.* **266** (1968) 1196.

[52] J. Koryta, P. Vanysek, M. Brecina, *J. Electroanal. Chem.* **67** (1976) 263.

[53] P. Liljeroth, A. Mälkiä, V. J. Cunnane, A. K. Kontturi, K. Kontturi, *Langmuir* **16** (2000) 6667.

[54] A. Mälkiä, P. Liljeroth, A. K. Kontturi, K. Kontturi, *J. Phys. Chem. B* **105** (2001) 10884.

[55] K. Kontturi, L. Murtomäki, *J. Pharm. Sci.* **81** (1992) 970.

[56] F. Reymond, G. Steyaert, P. A. Carrupt, B. Testa, H. H. Girault, *Helv. Chim. Acta* **79** (1996) 101.

[57] F. Reymond, G. Steyaert, A. Pagliara, P. A. Carrupt, B. Testa, H. Girault, *Helv. Chim. Acta* **79** (1996) 1651.

[58] F. Reymond, P. A. Carrupt, B. Testa, H. H. Girault, *Chem.-Eur. J.* **5** (1999) 39.

[59] F. Reymond, V. Chopineaux-Courtois, G. Steyaert, G. Bouchard, P. A. Carrupt, B. Testa, H. H. Girault, *J. Electroanal. Chem.* **462** (1999) 235.

[60] F. Reymond, G. Steyaert, P. A. Carrupt, D. Morin, J. P. Tillement, H. H. Girault, B. Testa, *Pharm. Res.* **16** (1999) 616.

[61] G. Caron, G. Steyaert, A. Pagliara, F. Reymond, P. Crivori, P. Gaillard, P. A. Carrupt, A. Avdeef, J. Comer, K. J. Box, H. H. Girault, B. Testa, *Helv. Chim. Acta* **82** (1999) 1211.

[62] G. Caron, F. Reymond, P. A. Carrupt, H. H. Girault, B. Testa, *Pharm. Sci. Technol. Today* **2** (1999) 327.

[63] V. Gobry, S. Ulmeanu, F. Reymond, G. Bouchard, P. A. Carrupt, B. Testa, H. H. Girault, *J. Am. Chem. Soc.* **123** (2001) 10684.

[64] J. Willner, W. E. Ford, J. W. Otwos, M. Calvin, *Nature* **280** (1979) 823.

[65] D. J. Fermin, H. D. Duong, Z. F. Ding, P. F. Brevet, H. H. Girault, *Electrochem. Commun.* **1** (1999) 29.

[66] R. Lahtinen, D. J. Fermin, K. Kontturi, H. H. Girault, *J. Electroanal. Chem.* **483** (2000) 81.

[67] I. Bustero, Y. F. Cheng, J. C. Mugica, T. Fernandez-Otero, A. F. Silva, D. J. Schiffrin, *Electrochim. Acta* **44** (1998) 29.

[68] L. Tomaszewski, G. Lagger, H. H. Girault, *Anal. Chem.* **71** (1999) 837–841.

[69] G. Lagger, L. Tomaszewski, M. D. Osborne, B. J. Seddon, H. H. Girault, *J. Electroanal. Chem.* **451** (1998) 29.

[70] R. M. Lahtinen, D. J. Fermin, H. Jensen, K. Kontturi, H. H. Girault, *Electrochem. Commun.* **2** (2000) 230.

[71] E. V. Dehmlow, S. S. Dehmlow, Phase transfer catalysis, 1st Edition, Verlag Chemie, Weinheim, 1980.

[72] V. J. Cunnane, D. J. Schiffrin, C. Beltran, G. Geblewicz, T. Solomon, *J. Electroanal. Chem.* **247** (1988) 203.

[73] Y. Cheng, D. J. Schiffrin, *In preparation* .

[74] M. Guainazzi, G. Silvestri, G. Serravalle, *J. Chem. Soc., -Chem. Commun.* **6** (1975) 200.

[75] V. J. Cunnane, U. Evans, *J. Chem. Soc. -Chem. Commun.* (1998) 2163.

[76] M. Platt, R. A. W. Dryfe, E. P. L. Roberts, *Electrochem. Commun.* **20** (2002) 2324.

[77] P. Liljeroth, C. Johans, K. Kontturi, J. A. Manzanares, *J. Electroanal. Chem.* **483** (2000) 37.

[78] F. Silva, M. J. Sousa, C. M. Pereira, *Electrochim. Acta* **42** (1997) 3095.

[79] V. Mareček, H. Jänchenova, M. Colombini, P. Papoff, *J. Electroanal. Chem.* **217** (1987) 213.

[80] B. Hundhammer, S. K. Dhawan, A. Bekele, H. T. Seidlitz, *J. Electroanal. Chem.* **217** (1987) 253.

[81] B. Hundhammer, S. Wilke, *J. Electroanal. Chem.* **266** (1989) 133.

[82] B. Hundhammer, T. Solomon, T. Zerihun, M. Abegaz, A. Bekele, K. Graichen, *J. Electroanal. Chem.* **371** (1994) 1.

[83] D. M. Mitrinovic, Z. J. Zhang, S. M. Williams, Z. Q. Huang, M. L. Schlossman, *J. Phys. Chem. B* **103** (1999) 1779.

[84] A. M. Tikhonov, D. M. Mitrinovic, M. Li, Z. Q. Huang, M. L. Schlossman, *J. Phys. Chem. B* **104** (2000) 6336.

[85] M. L. Schlossman, M. Li, D. M. Mitrinovic, A. M. Tikhonov, *High Perform. Polym.* **12** (2000) 551.

[86] J. Strutwolf, A. L. Barker, M. Gonsalves, D. J. Caruana, P. R. Unwin, D. E. Williams, J. R. P. Webster, *J. Electroanal. Chem.* **483** (2000) 163.

[87] A. Trojanek, P. Krtil, Z. Samec, *J. Electroanal. Chem.* **517** (2001) 77.

[88] D. A. Higgins, R. M. Corn, *J. Phys. Chem.* **97** (1993) 489.

[89] J. C. Conboy, J. L. Daschbach, G. L. Richmond, *J. Phys. Chem.* **98** (1994) 9688.

[90] A. A. T. Luca, P. Hebert, P. F. Brevet, H. H. Girault, *J. Chem. Soc. -Faraday Trans* **91** (1995) 1763.

[91] M. J. Crawford, J. G. Frey, T. J. VanderNoot, Y. G. Zhao, *J. Chem. Soc. -Faraday Trans* **92** (1996) 1369.

[92] H. F. Wang, E. Borguet, K. B. Eisenthal, *J. Phys. Chem. B* **102** (1998) 4927.

[93] Q. Du, E. Freysz, Y. R. Shen, *Science* **264** (1994) 826.

[94] M. C. Messmer, J. C. Conboy, G. L. Richmond, *J. Am. Chem. Soc.* **117** (1995) 8039.

[95] D. E. Gragson, G. L. Richmond, *Langmuir* **117** (1995) 8039.

[96] P. B. Miranda, Y. R. Shen, *J. Phys. Chem. B* **103** (1999) 3292.

[97] L. F. Scatena, M. G. Brown, G. L. Richmond, *Science* **292** (2001) 908.

[98] G. L. Richmond, *Annu. Rev. Phys. Chem.* **52** (2001) 357.

[99] L. F. Scatena, G. L. Richmond, *J. Phys. Chem. B* **105** (2001) 11240.

[100] D. Michael, I. Benjamin, *J. Chem. Phys.* **114** (2001) 2817.

[101] K. Schweighofer, I. Benjamin, *J. Chem. Phys.* **112** (2000) 1474.

[102] D. Michael, I. Benjamin, *J. Electroanal. Chem.* **450** (1998) 335.

[103] I. Benjamin, *Annu. Rev. Phys. Chem.* **48** (1997) 407.

[104] K. J. Schweighofer, I. Benjamin, *J. Electroanal. Chem.* **391** (1995) 1.

[105] D. Michael, I. Benjamin, *J. Phys. Chem.* **99** (1995) 1530.

[106] I. Benjamin, *Science* **261** (1993) 1558.

[107] I. Benjamin, *J. Chem. Phys.* **97** (1992) 1432.

[108] E. J. Verwey, K. F. Niessen, *Phil. Mag.* **28** (1939) 435.

[109] C. Gavach, P. Seta, B. d'Epenoux, *J. Electroanal. Chem.* **83** (1977) 225.

[110] Z. Samec, V. Mareček, D. Homolka, *J. Chem. Soc., -Faraday Trans* **77** (1984) 277.

[111] Z. Samec, V. Mareček, D. Homolka, *J. Electroanal. Chem.* **187** (1985) 31.

[112] H. H. Girault, D. J. Schiffrin, *J. Electroanal. Chem.* **150** (1983) 43.

[113] C. M. Pereira, W. Schmickler, F. Silva, M. J. Sousa, *J. Electroanal. Chem.* **436** (1997) 9.

[114] C. M. Pereira, W. Schmickler, A. F. Silva, M. J. Sousa, *Chem. Phys. Lett.* **268** (1997) 13.

[115] D. J. Henderson, W. Schmickler, *J. Chem. Soc. -Faraday Trans* **92** (1996) 3839.

[116] T. Huber, O. Pecina, W. Schmickler, *J. Electroanal. Chem.* **467** (1999) 203.

[117] S. Frank, W. Schmickler, *J. Electroanal. Chem.* **483** (2000) 18.

[118] Z. Samec, T. Kakiuchi, Charge transfer kinetics at the water-organic solvent phase boundaries, H. Gerisher, C. W. Tobias (Eds.), Vol. 4 of *Advances in electrochemical science and engineering*, Weinheim, 1995, pp. 300–361.

[119] A. J. Parker, *Electrochim. Acta* **21** (1976) 671.

[120] T. Kakiuchi, Y. Takasu, *J. Electroanal. Chem.* **365** (1994) 293.

[121] L. Tomaszewski, F. Reymond, P. F. Brevet, H. H. Girault, *J. Electroanal. Chem.* **483** (2000) 135.

[122] F. Reymond, G. Lagger, P. A. Carrupt, H. H. Girault, *J. Electroanal. Chem.* **451** (1998) 59.

[123] F. Reymond, P. A. Carrupt, H. H. Girault, *J. Electroanal. Chem.* **449** (1998) 49.

[124] A. Sabela, V. Mareček, J. Koryta, Z. Samec, *Collect. Czech. Chem. Commun.* **59** (1994) 1287.

[125] T. Kakiuchi, *J. Colloid Interface Sci.* **156** (1993) 406.

[126] T. Kakiuchi, M. Senda, *J. Electroanal. Chem.* **300** (1991) 431.

[127] C. Gavach, B. d'Epenoux, F. Henry, *J. Electroanal. Chem.* **64** (1975) 107.

[128] Z. Samec, V. Mareček, J. Koryta, M. W. Khalil, *J. Electroanal. Chem.* **83** (1977) 393.

[129] W. E. Bronner, O. R. Melroy, R. P. Buck, *J. Electroanal. Chem.* **162** (1984) 263.

[130] T. Kakiuchi, J. Noguchi, M. Kotani, M. Senda, *J. Electroanal. Chem.* **296** (1990) 517.

[131] T. Wandlowski, V. Mareček, K. Holub, Z. Samec, *J. Phys. Chem.* **93** (1989) 8204.

[132] P. D. Beattie, A. Delay, H. H. Girault, *Electrochim. Acta* **40** (1995) 2961.

[133] Z. Samec, *J. Electroanal. Chem.* **103** (1979) 1.

[134] H. H. Girault, D. J. Schiffrin, *J. Electroanal. Chem.* **244** (1988) 15.

[135] R. A. Marcus, *J. Phys. Chem* **94** (1990) 1050.

[136] R. A. Marcus, *J. Phys. Chem* **94** (1990) 4152.

[137] R. A. Marcus, *J. Phys. Chem* **94** (1990) 7742.

[138] R. A. Marcus, *J. Phys. Chem.* **95** (1991) 2010.

[139] I. Benjamin, Y. I. Kharkats, *Electrochim. Acta* **44** (1998) 133.

[140] I. Benjamin, *J. Phys. Chem.* **95** (1991) 6675.

[141] W. Schmickler, *J. Electroanal. Chem.* **428** (1997) 123.

[142] B. Quinn, K. Kontturi, *J. Electroanal. Chem.* **483** (2000) 124.

[143] M. Tsionsky, A. J. Bard, M. V. Mirkin, *J. Am. Chem. Soc.* **119** (1997) 10785–10792.

[144] Z. Ding, B. Quinn, A. J. Bard, *J. Phys. Chem. B* **105** (2001) 6367.

[145] S. N. Tan, R. A. W. Dryfe, H. H. Girault, *Helv. Chim. Acta* **77** (1994) 231.

[146] Y. T. Kong, S. Imabayashi, T. Kakiuchi, *Anal. Sci.* **14** (1998) 121.

[147] C. Forssten, J. Strutwolf, D. E. Williams, *Electrochem. Commun.* **3** (2001) 619.

[148] C. Forssten, K. Kontturi, L. Murtomäki, H. C. Hailes, D. E. Williams, *Electrochem. Commun.* **3** (2001) 379.

[149] R. Lahtinen, Catalysis at liquid-liquid interfaces -The electrochemical approach. *Ph.D. thesis*, Helsinki University of Technology (April 2000).

[150] B. M. Quinn, P. Liljeroth, K. Kontturi, *J. Am. Chem. Soc.* **124** (2002) 12915.

[151] S. Efrima, *Hetero. Chem. Rev.* **1** (1994) 339.

[152] L. Zeiri, S. Efrima, M. Deutsch, *Langmuir* **12** (1996) 5180.

[153] O. Younes, L. Zeiri, S. Efrima, M. Deutsch, *Langmuir* **13** (1997) 1767.

[154] G. Gunawardena, G. Hills, I. Montenegro, B. Scharifker, *J. Electroanal. Chem.* **138** (1982) 255.

[155] B. Scharifker, G. Hills, *Electrochim. Acta* **28** (1983) 879.

[156] B. R. Scharifker, J. Mostany, *J. Electroanal. Chem.* **177** (1984) 13.

[157] R. Aveyard, J. H. Clint, *J. Chem. Soc., -Faraday Trans* **92** (1996) 85.

[158] F. Bresme, N. Quirke, *Phys. Chem. Chem. Phys.* **1** (1999) 2149.

[159] F. Bresme, N. Quirke, *J. Chem. Phys.* **110** (1999) 3536.

[160] F. Bresme, N. Quirke, *Phys. Rev. Lett.* **80** (1998) 3791.

[161] S. Li, C. W. Macosko, H. S. White, *Science* **259** (1993) 957.

[162] Y. Sun, E. Ruckenstein, *Synth. Metals* **82** (1996) 5.

[163] P. Novak, K. Muller, K. S. V. Santhanam, O. Hass, *Chem. Rev.* **97** (1997) 207.

[164] J. S. Miller, *Adv. Mater* **5** (1993) 587.

[165] J. S. Miller, *Adv. Mater* **5** (1993) 671.

[166] J. D. Moreno, M. L. Marcos, F. Agulló-Rueda, R. G.-L. abd R. J. Martín-Palma, J. M. Martinez-Duart, J. González-Velasco, *Thin Solid Films* **348** (1999) 152.

[167] K. Gorgy, F. Fusalba, U. Evans, K. Kontturi, V. J. Cunnane, *Synth. Met.* **125** (2001) 365.

[168] K. Maeda, H. Jänchenova, A. Lhotsky, I. Stibor, J. Budka, V. Mareček, *J. Electroanal. Chem.* **516** (2001) 103.

[169] J. L. Fransaer, R. M. Penner, *J. Phys. Chem. B* **103** (1999) 7643.

[170] M. Volmer, A. Weber, *Z. Phys. Chem.* **119** (1926) 277.

[171] R. Greef, R. Peat, L. M. Peter, D. Pletcher, J. Robinson, Instrumental techniques in electrochemistry, Ellis Horwood, Chichester, 1985.

[172] A. Milchev, *Contemporary Physics* **32** (1991) 321.

[173] M. Y. Abyaneh, *J. Electroanal. Chem* **530** (2002) 82.

[174] G. Nagy, G. Denuault, *J. Electroanal. Chem.* **433** (1997) 175.

[175] Y. Cao, P. C. Searson, A. C. West, *J. Electrochem. Soc* **148** (2001) C376.

[176] F. C. Frank, *Proc. R. Soc. London, Ser A* **201** (1950) 586.

[177] M. Avrami, *J. Chem. Phys.* **7** (1939) 1103.

[178] M. Sluyters-Rehbach, J. H. O. J. Wijenberg, E. Bosco, J. H. Sluyters, *J. Electroanal. Chem.* **236** (1987) 1.

[179] M. V. Mirkin, A. P. Nilov, *J. Electroanal. Chem.* **283** (1990) 35.

[180] L. Heerman, E. Matthijs, S. Langerock, *Electrochim. Acta* **47** (2001) 905.

[181] L. Heerman, A. Tarallo, *Electrochem. Commun.* **2** (2000) 85.

[182] L. Heerman, A. Tarallo, *J. Electroanal. Chem.* **470** (1999) 70.

[183] R. Gangopadhyay, A. De, *Chem. Mater.* **12** (2000) 608.

[184] M. Hepel, *Chem. Mater.* **145** (1998) 124.

[185] N. Cioffi, L. Torsi, L. Sabbatini, P. Zambonin, T. Bleve-Zacheo, *J. Electroanal. Chem.* **488** (2001) 42.

[186] N. Cioffi, L. Torsi, I. Losito, L. Sabbatini, P. G. Zambonin, T. Bleve-Zacheo, *Electrochim. Acta* **46** (2001) 4205.

[187] S. Tamil Selvan, J. P. Spatz, H.-A. Klok, M. Moeller, *Adv. Mater.* **10** (1998) 131.

[188] M. Moeller, J. P. Spatz, H.-A. Klok, A. Roesher, S. Moessmer, S. Tamil Selvan, *Macromol. Symp.* **117** (1997) 207.

[189] S. Tamil Selvan, *J. Chem. Soc. -Chem. Commun.* (1998) 351.

[190] S. Tamil Selvan, J. P. Spatz, H.-A. Klok, M. Moeller, G. H., T. C. W. (Eds.), Quantum dot materials for nonlinear optics applications, Kluwer Academic Press, 1997.

[191] Y. Zhou, H. Itoh, T. Uemura, K. Naka, Y. Chujo, *Langmuir* **18** (2002) 277.

[192] G. Beamson, D. Briggs, High resolution XPS for organic polymers, Wiley, London, 1992.

[193] L. Feigin, D. Svergun, Structure Analysis by Small-Angle X-Ray and Neutron Scattering, Plenum Press, New York, 1987.

[194] J. F. Moulder, W. F. Stickle, P. E. Sobol, K. D. Bomben, Handbook of X-ray photoelectron spectroscopy, J. Chastain, R. C. King Jr. (Eds.), Physical Electronics, Eden Prairie, 1995.

[195] J. Creighton, D. Eadon, *J. Chem. Soc. -Faraday Trans* **87** (1991) 3881.

[196] C. Visy, J. Lukkari, J. Kankare, *Synth. Met.* **69** (1995) 319.

[197] N. Sato, M. Rikukawa, K. Sanui, N. Ogata, *Synth. Met.* **101** (1999) 132.

[198] J. Roncali, *Chem. Rev.* **92** (1992) 711.

[199] V. Tsakova, S. Winkels, J. Schultze, *Electrochim. Acta* **46** (2000) 759.